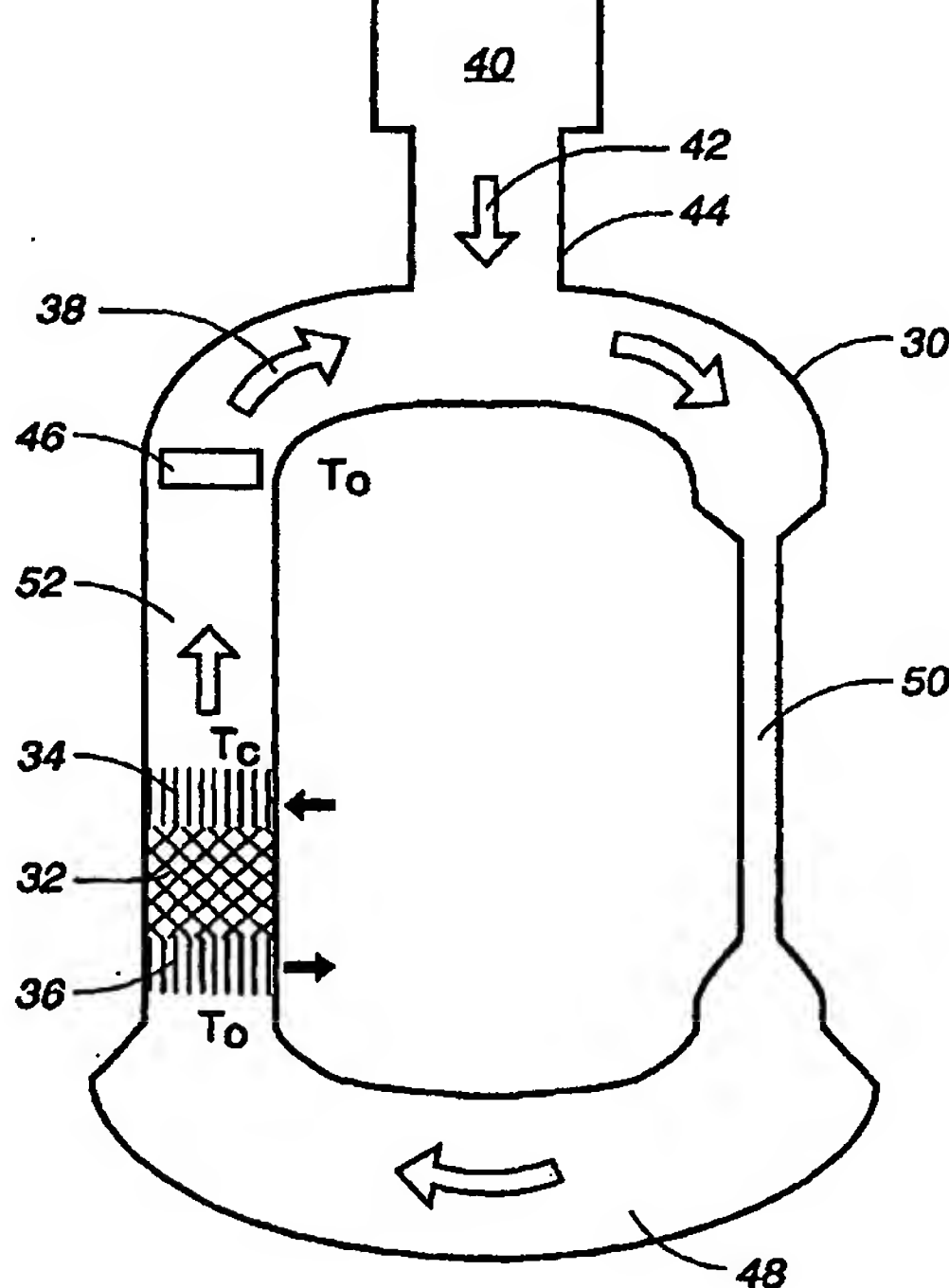


PCT

WORLD INTELLECTUAL PROPERTY ORGANIZATION
International Bureau



INTERNATIONAL APPLICATION PUBLISHED UNDER THE PATENT COOPERATION TREATY (PCT)

(51) International Patent Classification ⁷ :	A1	(11) International Publication Number:	WO 00/43639
F01B 29/10		(43) International Publication Date:	27 July 2000 (27.07.00)
(21) International Application Number:	PCT/US00/01308		
(22) International Filing Date:	19 January 2000 (19.01.00)		
(30) Priority Data:	<p>09/234,236 20 January 1999 (20.01.99) US</p>		
(71) Applicant:	THE REGENTS OF THE UNIVERSITY OF CALIFORNIA [US/US]; Business & Patent Law, MS D412, Los Alamos National Laboratory, P.O. Box 1663, Los Alamos, NM 87545 (US).		
(72) Inventors:	SWIFT, Gregory, W.; Rt. 5, Box 287-H, Santa Fe, NM 87501 (US). BACKHAUS, Scott, N.; 4627 Ridgeway, Los Alamos, NM 87544 (US). GARDNER, David, L.; 512 Brighton, Los Alamos, NM 87544 (US).		
(74) Agents:	WILSON, Ray, G. et al.; Business and Patent Law, MS D412, Los Alamos National Laboratory, P.O. Box 1663, Los Alamos, NM 87545 (US).		
(54) Title:	TRAVELING-WAVE DEVICE WITH MASS FLUX SUPPRESSION		
(57) Abstract	<p>A traveling-wave device is provided with the conventional moving pistons eliminated. Acoustic energy circulates in a direction through a fluid within a torus (30). A side branch may be connected to the torus for transferring acoustic energy into or out of the torus. A regenerator (32) is located in the torus with a first heat exchanger (34) located on a first side of the regenerator downstream of the regenerator relative to the direction of the circulating acoustic energy; and a second heat exchanger (36) located on an upstream side of the regenerator. The improvement is a mass flux suppressor (46) located in the torus to minimize time-average mass flux of the fluid. In one embodiment, the device further includes a thermal buffer column (70) in the torus to thermally isolate the heat exchanger that is at the operating temperature of the device.</p>		
(81) Designated States:	AE, AL, AM, AT, AU, AZ, BA, BB, BG, BR, BY, CA, CH, CN, CU, CZ, DE, DK, EE, ES, FI, GB, GE, GH, GM, HR, HU, ID, IL, IS, JP, KE, KG, KP, KR, KZ, LC, LK, LR, LS, LT, LU, LV, MD, MG, MK, MN, MW, MX, NO, NZ, PL, PT, RO, RU, SD, SE, SG, SI, SK, SL, TJ, TM, TR, TT, UA, UG, UZ, VN, YU, ZA, ZW, ARIPO patent (GH, GM, KE, LS, MW, SD, SL, SZ, TZ, UG, ZW), Eurasian patent (AM, AZ, BY, KG, KZ, MD, RU, TJ, TM), European patent (AT, BE, CH, CY, DE, DK, ES, FI, FR, GB, GR, IE, IT, LU, MC, NL, PT, SE), OAPI patent (BF, BJ, CF, CG, CI, CM, GA, GN, GW, ML, MR, NE, SN, TD, TG).		
Published	<p>With international search report. Before the expiration of the time limit for amending the claims and to be republished in the event of the receipt of amendments.</p>		
			

FOR THE PURPOSES OF INFORMATION ONLY

Codes used to identify States party to the PCT on the front pages of pamphlets publishing international applications under the PCT.

AL	Albania	ES	Spain	LS	Lesotho	SI	Slovenia
AM	Armenia	FI	Finland	LT	Lithuania	SK	Slovakia
AT	Austria	FR	France	LU	Luxembourg	SN	Senegal
AU	Australia	GA	Gabon	LV	Latvia	SZ	Swaziland
AZ	Azerbaijan	GB	United Kingdom	MC	Monaco	TD	Chad
BA	Bosnia and Herzegovina	GE	Georgia	MD	Republic of Moldova	TG	Togo
BB	Barbados	GH	Ghana	MG	Madagascar	TJ	Tajikistan
BE	Belgium	GN	Guinea	MK	The former Yugoslav Republic of Macedonia	TM	Turkmenistan
BF	Burkina Faso	GR	Greece	ML	Mali	TR	Turkey
BG	Bulgaria	HU	Hungary	MN	Mongolia	TT	Trinidad and Tobago
BJ	Benin	IE	Ireland	MR	Mauritania	UA	Ukraine
BR	Brazil	IL	Israel	MW	Malawi	UG	Uganda
BY	Belarus	IS	Iceland	MX	Mexico	US	United States of America
CA	Canada	IT	Italy	NE	Niger	UZ	Uzbekistan
CF	Central African Republic	JP	Japan	NL	Netherlands	VN	Viet Nam
CG	Congo	KE	Kenya	NO	Norway	YU	Yugoslavia
CH	Switzerland	KG	Kyrgyzstan	NZ	New Zealand	ZW	Zimbabwe
CI	Côte d'Ivoire	KP	Democratic People's Republic of Korea	PL	Poland		
CM	Cameroon	KR	Republic of Korea	PT	Portugal		
CN	China	KZ	Kazakhstan	RO	Romania		
CU	Cuba	LC	Saint Lucia	RU	Russian Federation		
CZ	Czech Republic	LI	Liechtenstein	SD	Sudan		
DE	Germany	LK	Sri Lanka	SE	Sweden		
DK	Denmark	LR	Liberia	SG	Singapore		
EE	Estonia						

TRAVELING-WAVE DEVICE WITH MASS FLUX SUPPRESSION

STATEMENT REGARDING FEDERAL RIGHTS

This invention was made with government support under Contract No. W-7405-ENG-36 awarded by the U.S. Department of Energy. The government has certain rights in the invention.

5

FIELD OF THE INVENTION

The present invention relates generally to traveling-wave engines and refrigerators, and, more particularly, to traveling-wave engines and refrigerators that perform as Stirling engines and refrigerators.

10

BACKGROUND OF THE INVENTION

There are a number of important antecedents to this invention. The most important antecedents are Stirling engines and refrigerators, a century old. An important step in the elimination of moving parts from Stirling engines and 15 refrigerators came in 1969, when William Beale invented the "free-piston" variety of Stirling devices, in which the crankshaft and linkages were replaced by gas springs, so that gas spring constants and piston masses could be chosen to cause resonant motion of the pistons with the desired frequency, amplitudes, and phases.

20

Ceperley, "Gain and efficiency of a short traveling-wave heat engine," 77

J. Acoust. Soc. Am., pp. 1239-1294 (1985) suggested that the essence of

Stirling engines and refrigerators is a regenerator (and adjacent heat

exchangers) in which the pressure and velocity oscillations are substantially in phase, reminiscent of an acoustic traveling-wave, and hence that an acoustic

25

network with essentially toroidal topology containing the Stirling heat-exchange components can provide such phasing. Ceperley claimed that efficiencies near 80% of the Carnot efficiency are in principle possible with such configurations.

Ceperley's contribution could be seen as an extension of Beale's, in that

Ceperley uses gas inertia effects in addition to Beale's gas spring effects, thereby eliminating the massive pistons of Beale's invention. Other related teachings by Ceperley are set out in U.S. Patents 4,113,380, issued September 19, 1978, and 4,355,517, issued October 26, 1982. However, Ceperley
5 presented no teachings on how to realize a practical device.

The conventional orifice pulse tube refrigerator (OPTR) (Radebaugh, "A review of pulse tube refrigeration," 35 Adv. Cryogenic Eng., pp. 843-844 (1992)) operates thermodynamically like a Stirling refrigerator, but with the cold moving parts replaced by passive components: a thermal buffer column known as the
10 pulse tube, and a dissipative acoustic impedance network. The efficiency \dot{Q}_C/\dot{W} of an OPTR is fundamentally limited by the temperature ratio T_C/T_0 , which is lower than the Carnot value $T_C/(T_0 - T_C)$ because of the inherent irreversibility in the dissipative acoustic impedance network. T is temperature, \dot{Q}_C is heat, \dot{W} is work, and the subscripts 0, and C refer to ambient and cold, respectively. The
15 OPTR can be regarded as another means to eliminate moving parts from Stirling devices. However, the efficiency of an OPTR is fundamentally less than that of a Stirling device, and the OPTR is only applicable to refrigerators.

Conventional OPTRs have long used the thermal buffer column known as a pulse tube, but until recently this component carried substantial heat leak.
20 However, using a tapered tube, as described in U.S. Patent Application S.N. 08/975,766, filed November 21, 1997, can reduce the heat leak along such a thermal buffer column to as little as 5% of the cooling power of a OPTR. Thermal buffer columns have been used in two-piston Stirling refrigerators as well as in OPTRs, but not in Stirling engines.
25 In the context of double-inlet OPTRs, Gedeon, "DC gas flows in Stirling and pulse-tube cryocoolers," in Ross ed., Cryocoolers 9, pp. 385-392 (Plenum, NY 1997) discusses how nonzero time-averaged mass flux \dot{M} can arise in Stirling and pulse-tube cryocoolers whenever a closed-loop path exists for steady mass flux. It is essential that \dot{M} through a Stirling engine or refrigerator
30 be near zero, to prevent a large steady energy flux $\dot{M}c_p(T_0 - T_C)$ from adding an

unwanted thermal load to the cold heat exchanger of a refrigerator, or to prevent a large steady energy flux $\dot{M}c_p(T_H - T_0)$ from removing a large amount of heat from the hot heat exchanger of an engine---in either case, reducing the efficiency. Here c_p is the gas isobaric specific heat per unit mass.

5 Another, less directly related antecedent to this invention is the set of prior thermoacoustic engines and refrigerators developed in the past 20 years at Los Alamos National Laboratory and elsewhere. These operate on an intrinsically irreversible cycle, using nearly standing-wave phasing between gas pressure oscillations and velocity oscillations and using deliberately imperfect thermal
10 contact in the stack (which might otherwise be mistaken for a regenerator). The intrinsic irreversibility and other practical issues have thus far limited the best standing-wave thermoacoustic engines and refrigerators to below 25% of the Carnot efficiency.

15 Various objects, advantages and novel features of the invention will be set forth in part in the description which follows, and in part will become apparent to those skilled in the art upon examination of the following or may be learned by practice of the invention. The objects and advantages of the invention may be realized and attained by means of the instrumentalities and combinations particularly pointed out in the appended claims.

20

SUMMARY OF THE INVENTION

To achieve the foregoing and other objects, and in accordance with the purposes of the present invention, as embodied and broadly described herein, the present invention includes a pistonless Stirling device. Acoustic energy
25 circulates in a direction through a fluid within a torus. In one embodiment, a side branch is connected to the torus for transferring acoustic energy into or out of the torus. A regenerator is located in the torus with a first heat exchanger located on a first side of the regenerator downstream of the regenerator relative to the direction of the circulating acoustic energy; and a second heat exchanger
30 located on a second side of the regenerator, where one of the heat exchangers is at an operating temperature and the other one of the heat exchangers is at

ambient temperature. The improvement herein comprises a mass flux suppressor located in the torus to minimize time averaged mass flux of the fluid. In one embodiment, the device further includes a thermal buffer column adjacent to the heat exchanger at the operating temperature to thermally isolate the heat 5 exchanger at the operating temperature.

BRIEF DESCRIPTION OF THE DRAWINGS

The accompanying drawings, which are incorporated in and form a part of the specification, illustrate embodiments of the present invention and, together 10 with the description, serve to explain the principles of the invention. In the drawings:

FIGURES 1A and 1B schematically depict the heat-exchange components of a prior art Stirling-cycle refrigerator and accompanying phasor diagram, respectively.

15 FIGURES 2A and 2B schematically depict the heat-exchange components of a prior art Stirling-cycle engine and accompanying phasor diagram.

FIGURE 3 schematically depicts one embodiment of a Stirling-cycle refrigerator according to the present invention.

20 FIGURE 4 schematically depicts one embodiment of a Stirling-cycle engine according to the present invention.

FIGURES 5A and 5B depict electrical circuit analogues for basic aspects of the present invention.

FIGURE 6 is a cross-sectional view of a refrigerator version of the present 25 invention with a diaphragm mass flux suppressor.

FIGURE 7 graphically depicts the power flows as a function of the cold heat exchanger temperature T_C for the refrigerator shown in Figure 6.

FIGURE 8 is a cross-sectional view of an engine version of the present invention with a hydrodynamic mass flux suppressor.

30 FIGURE 9 graphically depicts temperature profiles within the regenerator of the engine shown in FIGURE 8.

FIGURES 10A and 10B schematically illustrate asymmetric mass flux through a hydrodynamic mass flux suppressor.

FIGURE 11A graphically depicts the efficiencies of the engine shown in FIGURE 8 at $T_H=525^{\circ}\text{C}$.

5 FIGURE 11B graphically depicts the efficiencies of the engine shown in FIGURE 8 with $|p_1|/p_m=0.05$.

FIGURES 12A and 12B are a cross-sectional side view and a top view, respectively, of a variable slit mass flux suppressor for use in the present invention.

10 FIGURE 13A schematically depicts a heat pump adaptation of the refrigerator shown in FIGURE 3.

FIGURE 13B schematically depicts the refrigerator shown in FIGURE 3 driven by the engine shown in FIGURE 4.

15 FIGURE 13C schematically depicts a heat-driven refrigerator located in a single torus.

FIGURE 13D schematically depicts a plurality of refrigerators shown in FIGURE 3 connected in parallel and driven from a single source.

DETAILED DESCRIPTION

20 In accordance with the present invention, a new class of engines and refrigerators operate thermodynamically like Stirling engines and refrigerators, but all moving parts are eliminated by using acoustic phenomena in place of the pistons that have previously been used in Stirling devices. Thus, both the efficiency advantage of the Stirling cycle (whose inherent limit is the Carnot efficiency) and the no-moving-parts simplicity/reliability advantage of intrinsically irreversible thermoacoustics are obtained in these devices.

25 The essential components of a Stirling refrigerator 10 and a Stirling engine 20, shown in Figures 1A and 2A, are regenerators 12, each with two adjacent heat exchangers 16, 18. A gas (or other thermodynamically active fluid) 30 is made to experience pressure oscillations and displacement oscillations throughout these components, with phasing such that acoustic power enters the

components at the ambient-temperature end T_0 and leaves at the other end at cold temperature T_C , or hot temperature T_H , as shown by the long broad arrows in Figures 1A and 2A. Regenerators 12 have heat capacity, and the gas passages within regenerators 12 have hydraulic radii smaller than the thermal penetration depth in the gas.

To consider the thermodynamic cycle quantitatively, assume the essential physics to be spatially one dimensional, with x specifying the coordinate along the direction of oscillatory gas motion. Conventional counterclockwise phasor notation is used, so that time-dependent variables are expressed as

$$\xi(x, t) = \xi_m(x) + \text{Re}[\xi_1(x)e^{i\omega t}] \quad (1)$$

10

with the mean value ξ_m real and independent of time t , and with $\xi_1(x)$ complex to account for both the magnitude and phase of the oscillation, which occurs at angular frequency $\omega = 2\pi f$, where f is the ordinary frequency. An acoustical point of view is presented, using the vocabulary of acoustic resistance,

15 inertance, compliance, and transmission line to discuss the lumped and distributed impedances associated with the components of the engine or refrigerator. This approach has been successful previously, even within regenerators (see, e.g., Swift et al., "Simple harmonic analysis of regenerators," 10 Journal of Thermophysics and Heat Transfer, pp. 652-662 (1996)). The present approach focuses primarily on conventional acoustic variables: pressure amplitude p_1 and volumetric velocity U_1 . The positive direction for x and U_1 is taken as the direction of positive acoustic power flow.

20 Features of phasor diagrams for efficient Stirling engines and refrigerators are shown in Figures 1B and 2B. The capitalized subscripts on variable such as p_1 and U_1 correspond to the locations labeled with T having the same subscripts in Figures 1A and 2A and subsequent Figures. The arbitrary convention is adopted that the phases of the pressure at the refrigerator's cold heat exchanger (e.g., heat exchanger 16, Figure 1A) and the engine's hot heat exchanger (e.g., heat exchanger 18, Figure 1A) are zero, so p_{1C} in Figure 1B

and p_{1H} in Figure 2B fall on the real axis. Typically the pressure drop across the heat exchangers is negligible compared to that across the regenerator, which is in turn small compared to $|p_1|$, so p_{10} must lie close to p_{1C} or p_{1H} , as shown in Figures 1B and 2B.

5 Typically the time-averaged energy flux through the regenerator is small. Applying energy conservation to cold heat exchanger 16 in Figure 1A then shows that the cooling power \dot{Q}_C , shown by the short heavy arrow, is about equal to the total acoustic power flowing out of the cold heat exchanger in the positive x direction, $\dot{W}_C = \frac{1}{2} \operatorname{Re}[p_{1C} \tilde{U}_{1C}] = \frac{1}{2} |p_{1C}| |U_{1C}| \cos \theta_C$, shown by the long arrow in Figure 1A, where θ_C is the phase angle between p_{1C} and U_{1C} . In fact, heat leaks can flow to the cold heat exchanger, so the acoustic power is an upper bound on the actual cooling power:

$$\dot{Q}_C \leq \frac{1}{2} \operatorname{Re}[p_{1C} \tilde{U}_{1C}] \quad (2)$$

In Figure 1A, in order to achieve positive cooling power, acoustic power must flow in the direction shown with the long arrows, in the positive x direction, 15 so U_{10} and U_{1C} must lie in the right half plane in Figure 1B. An idealized regenerator might be imagined with negligible entrained gas volume, so that $\rho_m U_1$ would be independent of x in the regenerator (where ρ_m is the gas mean density), and in particular the phase of U_1 would be constant throughout the regenerator. However, it is well known that nonzero gas volume in the 20 regenerator causes x dependence in U_1 , proportional to the local gas volume and to $i\omega p_1$. This leads to a spread in phase of U_1 through the system, with U_1 at small x (i.e. toward ambient heat exchanger 18) leading. The most efficient regenerator operation occurs when $|U_1|$ is as small as possible for a given 25 cooling power, because this leads to minimal viscous pressure drop across the regenerator and minimal energy flux through the regenerator due to imperfect thermal contact in the regenerator. To achieve small $|U_1|$ for a given \dot{W}_C , U_1 should be nearly in phase with p_1 , so the phase of p_1 should fall somewhere

between the phases of U_{1C} and U_{10} . Viscous pressure drop occurs throughout the regenerator, so $p_{10} - p_{1C}$ must be in phase with (parallel to) some weighted average of U_1 in the regenerator. Both $|U_1|$ and viscosity are highest at the regenerator's ambient end T_0 , so the weighted average is typically dominated by 5 U_{10} , usually ensuring that p_{10} leads p_{1C} . All these features are illustrated in Figure 1B.

Much of the above discussion also applies directly to an engine. As noted above, the components of a Stirling engine, shown in Figure 2A, are nearly identical to those of a Stirling refrigerator. The main difference is that regenerator 10 12 in the engine produces work while the refrigerator's regenerator 12 absorbs work. This difference can be seen in the phasor diagram of Figure 2B. With $\theta_0 < 90^\circ$, acoustic power flows into the ambient side of regenerator 12. The mean temperature $T_m(x)$ rises from T_0 to T_H through regenerator 12. This increase in T_m causes ρ_m to fall. Since the first-order mass flux $\rho_m U_1$ is nearly 15 independent of x , the volume velocity increases, so $|U_{1H}| > |U_{10}|$. In addition, the volume of gas entrained in the regenerator causes the phase of U_1 to rotate in a similar fashion as in the refrigerator. These two effects locate U_{1H} relative to U_{10} in Figure 2B. The amplification of the acoustic power is indicated by

$$\frac{1}{2} |p_{1H}| |U_{1H}| \cos \theta_H > \frac{1}{2} |p_{10}| |U_{10}| \cos \theta_0.$$

20 Since the time-averaged energy flux through regenerator 12 is small, the acoustic power flowing out of hot heat exchanger 18 is nearly equal to the heat flowing into hot heat exchanger 18. Again, heat leaks and other losses reduce this power making Q_H an upper bound on the acoustic power, i.e.,

$$\frac{1}{2} \operatorname{Re}(p_{1H} \tilde{U}_{1H}) \leq Q_H. \text{ The location of } p_{10} \text{ relative to } p_{1H} \text{ is due to viscous}$$

25 pressure drop within regenerator 12, with the difference $p_{10} - p_{1H}$ proportional to a weighted average of U_1 through regenerator 12. Similar to the refrigerator, the

viscous effects are largest at the hot end of regenerator 12, where $|U_1|$ is largest and viscosity is largest. Hence, with U_{1H} dominating, p_{10} lags p_{1H} slightly.

Returning now to the refrigerator, as discussed above, the acoustic power

$$\dot{W}_C = \frac{\omega}{2\pi} \int_0^{2\pi/\omega} p(t)U(t)dt = \frac{1}{2} \operatorname{Re}[p_{1C}\bar{U}_{1C}] \quad (3)$$

flows out of the refrigerator's 10 cold heat exchanger 16. As taught by Ceperley,
5 ideally this acoustic power should be transmitted without loss to the ambient heat
exchanger. To accomplish this, Ceperley prescribed a full-wavelength torus
transmitting the acoustic wave. But, in accordance with one aspect of the
present invention, it is advantageous to use a much shorter sub-wavelength
torus 30, shown schematically in Figure 3, because it is more compact.

10 Figure 3 shows an embodiment of a refrigerator version of the present
invention. A torus 30 with total length less than a quarter of the acoustic
wavelength contains the Stirling refrigerator regenerator 32 and two heat
exchangers 34, 36. As used herein, the term "torus" means a pipe, tube, or the
like that defines a circulation path that is a loop that is circular or elongated,
15 having a cross-section for supporting an acoustic wave, preferably circular.
Acoustic power 38 circulates clockwise around torus 30, as shown by the long
arrows. Additional acoustic power 42 generated by acoustic device 40 (such as
an intrinsically irreversible thermoacoustic engine, a loudspeaker, a motor-driven
piston, or a traveling-wave engine) enters torus 30 from side branch 44, to make
20 up for acoustic power lost in regenerator 32 and elsewhere in the torus. As more
fully explained below, a mass flux suppressor 46 is located within torus 30 to
reduce the time-averaged mass flux \dot{M} substantially to zero.

In one embodiment, the flow resistance of mass flux suppressor 46,
shown in Figure 3, has a resistance R_M such that

$$p_{1C} - p_{1J} = R_M U_{1M}, \quad (4)$$

25 where subscript J signifies the location of the junction between torus 30 and
side branch 44. A compliance portion 48 of torus 30 ensures that the volumetric
velocity U_{1L} through an inertance portion 50 of torus 30 differs from that through
ambient heat exchanger 36:

$$U_{1L} = U_{10} + j \frac{\omega V_0}{\gamma p_m} p_{10} \quad (5)$$

where V_0 is the volume of the compliance portion 48 of torus 30, so that the pressure difference across inertance 50 is

$$p_{1J} - p_{10} = j\omega \frac{\rho_m l}{S} \left(U_{10} + j \frac{\omega V_0}{\gamma p_m} p_{10} \right) \quad (6)$$

where l and S are the length and area, respectively, of inertance 50. Taking the phasors at C, M, and 0 to be given and combining Equations (4) and (6) to 5 eliminate p_{1J} , a single complex equation is obtained in the unknowns R_M , V_0 , l , and S , generally with many possible solutions that enable a refrigerator to be built according to the present invention.

An embodiment of the engine version of the invention is shown schematically in Figure 4. Torus 60, whose total length is less than a quarter 10 wavelength, contains the Stirling engine's regenerator 62 and heat exchangers 64, 66. As shown by the long arrows 68, acoustic power circulates clockwise around torus 60. Surplus acoustic power 72 generated by the engine may be tapped off by side branch 74, and is available to perform useful work through acoustic device 76 (which could be a piezoelectric or electrodynamic transducer, 15 an orifice pulse tube refrigerator, or a refrigerator according to the present invention). Acoustic power 68 circulates around the torus and provides the input work to the ambient end T_0 of the Stirling engine. Therefore, this circulating work 68 replaces the ambient piston in a conventional Stirling engine. Mass-flux suppressor 75 again acts to reduce the time-averaged mass flux \dot{M} toward 20 zero. The analysis of short torus 60 is entirely parallel to Equations (4)-(6), and follows by merely replacing the subscript C with H .

The choice of an operating frequency for the devices shown in Figures 3 and 4 involves a compromise among many issues. High frequency leads to high power per unit volume of the device, because many thermodynamic cycles are 25 performed per unit time and because lengths of the device along propagation direction x scale approximately with wavelength, which is inversely proportional to frequency. On the other hand, low frequency eases the design and

construction of heat exchangers and regenerators, whose pore sizes scale approximately with thermal penetration depth, which is inversely proportional to the square root of the frequency.

The fact that acoustic power will naturally circulate clockwise around the tori of Figures 3 and 4, even though the tori are shorter than a quarter of an acoustic wavelength in exemplary embodiments, seems surprising. But consider the electrical circuits of Figures 5A and 5B, containing a resistance R, an inductance L, and a capacitance C, crudely analogous to the acoustic circuits of Figures 3 and 4, respectively. Resistance R is crudely analogous to the regenerator and heat exchangers, inductance L is analogous to the acoustic inertance, and capacitance C is analogous to the acoustic compliance.

Derivation of expressions for the ac currents in each component of the electrical circuits is straightforward, and allows further derivation of expressions for the electric power \dot{E} flowing at each location in the circuit. In these idealized circuits, no time-averaged power can be absorbed in the dissipationless inductor L nor flow into the dissipationless capacitor C. Ordinary ac circuit analysis easily yields the fed-back power

$$\dot{E}_F = \frac{1}{2} \operatorname{Re}[V_{1S} \tilde{I}_{1R}] = \frac{|V_{1S}|^2}{2R} \frac{\omega^2 LC(1 - \omega^2 LC)}{(1 - \omega^2 LC) + (\omega L/R)^2} \quad (7)$$

in Figure 5A, with the sign convention as shown in the figure. Hence, whenever $\omega^2 LC < 1$ the directions of time-averaged power flow are as shown by the arrows in Figure 5A; with positive electric power flowing clockwise around the circuit, analogous to the clockwise circulation of acoustic power in Figure 3. By energy conservation, the time-averaged power $\dot{E}_L - \dot{E}_F$ dissipated in the resistor must equal the time-averaged power $\dot{E}_S = \frac{1}{2} \operatorname{Re}[V_{1S} \tilde{I}_{1S}]$ flowing from the voltage source into the circuit. If the resistance R is negative, as shown in Figure 5B, power also circulates in the clockwise direction and the time-averaged power created in the negative resistance flows out of the circuit and into the voltage source.

It will be apparent to those skilled in the art of acoustics that inertances 50, 80 in Figures 3 and 4 may include significant compliance, and that

compliances 48, 78 in Figures 3 and 4 may include significant inertance. In fact, the function of these components may be served equally well by a short acoustic transmission line having distributed inertances and compliances throughout. For ease of discussion herein, the inertance and compliance are considered as
5 lumped components.

In the refrigerator of Figure 3, it is desirable to eliminate heat leaks from ambient to cold heat exchanger 34 in order to have the greatest possible cooling power. Similarly, in the engine of Figure 4 it is desirable to eliminate heat leaks from hot heat exchanger 66 to ambient in order to minimize the heater power
10 required to run the engine. Regenerators 32, 62 provide this thermal isolation on one side of cold heat exchanger 34 (in a refrigerator) or hot heat exchanger 66 (in an engine) in the present invention, as in all prior Stirling devices. On the other side of heat exchangers 34, 66, in accordance with one aspect of the
15 present invention, thermal buffer columns 52, 70, as shown in Figures 3 and 4, eliminate heat leaks. The gas in the thermal buffer columns 52, 70 can be thought of as an insulating piston, transmitting pressure and velocity from the cold 34 or hot 66 heat exchangers to ambient temperatures. The thermal buffer columns 52, 70 are exactly analogous to the pulse tube of an orifice pulse tube
20 refrigerator. Convective heat transfer of various forms could carry heat through thermal buffer columns 52, 70 between the cold 34 or hot 66 heat exchanges and ambient temperature. To eliminate gravitational convective heat transfer, thermal buffer columns 52, 70 should usually be oriented vertically with the cold end down, as shown in Figures 3 and 4. To eliminate gross shuttle convective
25 heat transfer, the thermal buffer columns 52, 70 should be longer than the peak-to-peak displacement amplitude of the gas within them. To maintain stratified oscillating plug flow in the thermal buffer column, its ends should be provided with flow straighteners (not shown). To eliminate streaming-driven convective heat transfer, thermal buffer columns 52, 70 should be tapered according to U.S. Patent Application 08/975,766, filed November 21, 1997, incorporated herein by
30 reference.

In another aspect of the present invention, the time-averaged mass flux \dot{M} around the torus (torus 30, Figure 3; torus 60, Figure 4) is controlled to be

near zero, to prevent a large steady energy flux $\dot{M}c_p(T_0 - T_C)$ from flowing to cold heat exchanger 34 in the refrigerator of Figure 3 or $\dot{M}c_p(T_H - T_0)$ flowing from hot heat exchanger 66 in the engine of Figure 4. In traditional Stirling engines and refrigerators, \dot{M} is exactly zero; otherwise, mass would accumulate 5 steadily on one or the other end of the system. Gedeon, *supra*, discusses how nonzero \dot{M} can arise in Stirling and pulse-tube cryocoolers whenever a closed-loop path exists for steady flow. Tori 30 (Figure 3) and 60 (Figure 4) clearly provide such a path; hence, the present invention minimizes \dot{M} .

To understand \dot{M} , extend the complex notation introduced in Equation 10 (1) to second order, by writing time-dependent variables as

$$\xi(x, t) = \xi_m(x) + \text{Re}[\xi_1(x)e^{i\omega t}] + \xi_2(x) \quad (8)$$

The new time-independent term, with subscript "2", is of great interest here.

Gedeon, *supra*, shows that the second-order time-average mass flux

$$\dot{M}_2 = \frac{1}{2} \text{Re}[\rho_1 \tilde{U}_1] + \rho_m U_2 \quad (9)$$

is of primary concern. In acoustics, such second-order mass flux is known as streaming. Gedeon, *supra*, further shows that $\frac{1}{2} \text{Re}[\rho_1 \tilde{U}_1] = \rho_m \dot{W}_2 / p_m$ in a 15 regenerator, where $\dot{W}_2 = \frac{1}{2} \text{Re}[p_1 \tilde{U}_1]$ is the acoustic power passing through the regenerator. Hence, $\frac{1}{2} \text{Re}[\rho_1 \tilde{U}_1]$ must be nonzero, and efficient regenerator operation requires that $U_2 = -\frac{1}{2} \text{Re}[\rho_1 \tilde{U}_1] / \rho_m = -\dot{W}_2 / p_m$. The consequences of ignoring this requirement can be severe. If $\dot{M}_2 \neq 0$, an undesired, streaming-induced heat current

$$\dot{Q}_{loss} \sim \dot{M}_2 c_p (T_0 - T_C), \text{ refrigerator} \quad (11)$$

$$\sim \dot{M}_2 c_p (T_H - T_0), \text{ engine} \quad (12)$$

20 flows through the system. (This heat can flow through either regenerators 32, 62

or thermal buffer columns 52, 70 in Figures 3 and 4, depending on the sign of \dot{M}_2 , with equally harmful effect.) For $U_2 = 0$, the ratio of \dot{Q}_{loss} to the ordinary regenerator loss \dot{H}_{reg} in the refrigerator is of the order of

$$\frac{\dot{Q}_{loss}}{\dot{H}_{reg}} \sim \frac{\gamma}{\gamma-1} \frac{(T_0 - T_C)}{T_0} \frac{\dot{W}_C}{\dot{H}_{reg}} \sim \frac{\gamma}{\gamma-1} \frac{(T_0 - T_C)}{T_C} \frac{\dot{Q}_C}{\dot{H}_{reg}}. \quad (13)$$

In the third expression, each of the three fractions is >1 for cryocoolers; hence
5 their product is $>>1$ and the unmitigated streaming-induced heat load would be
much greater than the ordinary regenerator loss in a cryocooler.

A laboratory version that embodies the present invention in a refrigerator is shown in Figure 6, which is topologically identical to that of Figure 3.

Refrigerator 80 was filled with 2.4 MPa argon and operated at 23 Hz, so that the
10 acoustic wavelength was 14 m. Refrigerator 80 was driven by an intrinsically
irreversible thermoacoustic engine 78. The dash-dot lines show local axes of
cylindrical symmetry. Acoustic power 114 circulates clockwise through inertance
82, compliance 84, and refrigerator parts 86 of the apparatus. Heavy flanges
102, 92 around first ambient heat exchanger 88 and second ambient heat
15 exchanger 96 contain water jackets. O-rings, most flanges, and bolts are
omitted for clarity.

Note that second ambient heat exchanger 96 is not necessary for the
operation of the invention. It does provide some flow straightening for the
ambient end of thermal buffer column 104. Water passages were included in
20 second ambient exchanger 96 because the parts were being reused from
unrelated tests involving a traditional OPTR configuration.

The heart of refrigerator 86, regenerator 98, was made of a 2.1 cm thick
stack of 400-mesh (i.e., 400 wires per inch) twilled-weave stainless-steel screens
punched at 6.1 cm diameter. The total weight of the screens in the regenerator
25 was 170 gm. The calculated value of the hydraulic radius of this regenerator
was approximately 12 μm , based on its geometry and weight. The hydraulic
radius is much smaller than the thermal penetration depth of the argon (100 μm
at 300 K), as required of a good regenerator. The stainless-steel pressure vessel
94 around regenerator 98 had a wall thickness of 1.4 mm. Thermal buffer

column 104 was a simple open cylinder, 3.0 cm id and 10.3 cm long, with 0.8 mm wall thickness. The diameter of buffer column 104 is much greater than the viscous penetration depth of the argon (90 μm at 300 K), and its length is greater than the 1-cm gas displacement amplitude in it at a typical operating point near
5 $|p_1|/p_m \sim 0.1$. At each end, a few 35-mesh copper screens (not shown) served as simple flow straighteners to help maintain oscillatory plug flow in thermal buffer column 104. The high density of argon enhances the gravitational stability of this plug flow, so that careful flow straightening and tapering were not embodied in this initial laboratory refrigerator. However, a gas providing more
10 power density, such as helium, may be used instead of argon, and the apparatus would be likely to need careful flow straightening and tapering for maximum performance. To obtain gravitational stability, the orientation of the refrigerator assembly was vertical, as shown in Figure 6.

For test purposes, cold heat exchanger 106 between regenerator 98 and
15 thermal buffer column 104 was a 1.8Ω length of NiCr ribbon wound zigzag on a fiberglass frame. Wires from the heater and a thermometer passed axially along the thermal buffer column to leak-tight electrical feedthroughs at room temperature. The two water-cooled heat exchangers (first ambient heat exchanger 88 and second ambient heat exchanger 96) were of shell-and-tube
20 construction, with the Reynolds number of order 10^4 at $|p_1|/p_m \sim 0.1$ in the argon inside the 1.7-mm-diameter, 18-mm long tubes. First ambient heat exchanger 88 had 365 such tubes, and second ambient heat exchanger 96 had 91.

Inertance 82 was a simple metal tube with 2.2 cm id and 21 cm length, with 7° cones, as shown in Figure 6, at both ends to reduce turbulent end
25 effects. Inertance 82 and refrigerator 86 components were sealed into flat plates above and below by rubber O-rings to enable easy modifications. The flat plates were held at a fixed separation by flange extensions and a cage of stout tubes (not shown) through which long bolts passed. Compliance 84 was half an ellipsoid with 2:2:1 aspect ratio, with a volume of 950 cm^3 .

30 Refrigerator 86 was configured first as shown in Figure 6, but without flexible diaphragm 108 (which may be a balloon-type diaphragm, or the like)

installed. At $|p_{1C}| / p_m = 0.068$ the refrigerator did not cool below 19°C, essentially the temperature of the cooling water supplied to the water-cooled heat exchangers that day. However, the pressure phasors were close to predictions and the refrigerator's cold temperature was very strongly
5 independent of heat load applied to the cold heat exchanger, e.g., at $|p_{1C}| / p_m = 0.07$, an applied load of 70 W raised T_C to only 35°C, as shown by the half-filled circles in Figure 7. Hence, the acoustic phenomena and gross cooling power were substantially as expected, and an extremely large nonzero \dot{M} was effectively keeping cold heat exchanger 106 thermally anchored to
10 ambient heat exchanger 88, overwhelming the otherwise satisfactory cooling power.

To show that the initial refrigerator performance shown as half-filled circles in Figure 7 was due to nonzero mass flux, flexible diaphragm 108 was installed above second ambient heat exchanger 96, as shown in Figure 6.
15 Flexible diaphragm 108 was selected to be acoustically transparent while blocking \dot{M} completely. With flexible diaphragm 108 in place, refrigerator 86 performed well, confirming that maintaining $\dot{M} = 0$ results in successful operation of this type of Stirling refrigerator. Flexible diaphragm 108 was operated at $|p_{10}| / p_m$ ranging from 0.04 to 0.10. In one set of measurements,
20 $|p_{1C}| / p_m = 0.054$ was maintained, while varying T_C from -115°C to 7°C by adjusting an electric heater power \dot{Q}_C at cold heat exchanger 106. ($T_0 = 13^\circ\text{C}$ throughout.) The filled symbols and lines in Figure 7 are the resulting measurements and calculations, respectively. The experimental points show the electric heater power \dot{Q}_C applied to cold heat exchanger 106 to maintain a given
25 T_C and the line is the corresponding calculation. Experimental points also show measured acoustic power $\dot{W}_{\text{sidebranch}}$ delivered from the side branch, and the long-dash line is the corresponding calculation. The short-dash line shows calculated values of recovered power (i.e., the acoustic power passing through flexible diaphragm 108).

The data depicted in Figure 7 show that the cooling power drops and the acoustic power supplied from the side branch rises as T_C decreases. The calculations, which are in reasonable agreement with the experiments, provide insight to the main causes of these trends. First, the calculated gross cooling

5 power $\dot{W}_C = \frac{1}{2} \operatorname{Re}[p_{1c}\bar{U}_{1c}]$ is nearly constant at 40 W, independent of T_C for these measurements. As discussed near Equation (2), under the most ideal circumstances this would be the cooling power. The decrease in calculated \dot{Q}_C below 40 W as T_C decreases is nearly proportional to $T_0 - T_C$ and is almost entirely due to heat flux through regenerator 98. The difference between

10 measured and calculated \dot{Q}_C is also proportional to $T_0 - T_C$, rising to 10 W at $T_C = -120^\circ\text{C}$. This could easily be due to a combination of ordinary heat leak through the insulation and streaming- or jet-driven convection in thermal buffer column 104. Second, under the most ideal circumstances---with 40 W of cooling power and with Carnot efficiency $\dot{Q}_C/\dot{W} = T_C/(T_0 - T_C)$ ---the required net

15 acoustic power would be $\dot{W} = (40 \text{ watts})(T_0 - T_C)/T_C$ which rises from zero at $T_C = T_0$ to 35 W at $T_C = -120^\circ\text{C}$. This accounts for most of the 40 W rise in calculated $\dot{W}_{\text{sidebranch}}$ with falling T_C in Figure 7. The measurements of $\dot{W}_{\text{sidebranch}}$ exceed calculations by roughly 30%, for unknown reasons. Calculations show that approximately 5 W of acoustic power is dissipated in second ambient heat

20 exchanger 96 under flexible barrier 108, 15 W is lost due to viscosity in regenerator 98 and adjacent heat exchangers 88, 106, and 10 W is dissipated in inertance 82.

If this were a traditional orifice pulse tube refrigerator, $\dot{W}_C = 40 \text{ W}$ would be dissipated in an orifice. In Figure 7, the calculated feedback acoustic power

25 $\dot{W}_{\text{recovered}}$, which is one aspect of this invention, is near 30 W; hence, approximately 75% of \dot{W}_C is recovered and fed back into the resonator through side branch 112. Note that at the highest temperatures $\dot{W}_{\text{recovered}}$ is comparable to $\dot{W}_{\text{sidebranch}}$. In other words, at these temperatures the toroidal configuration

reduces the acoustic power delivered from intrinsically irreversible thermoacoustic engine 78 to refrigerator 80 to roughly half of what it would be in a traditional orifice pulse tube refrigerator.

To demonstrate an engine embodiment of this invention, engine 120 shown in Figure 8 was constructed. It was filled with 3.1 MPa helium and operated at 5 70 Hz, with a corresponding acoustic wavelength of 14 m. The small circles in and below regenerator 122 indicate the location of some temperature sensors. Pressure sensors were also provided to measure P_{10} and P_{1H} . Most external hardware is shown in the figure, except for a cage of heavy bolts surrounding the sliding joints 148, the acoustic resonator, and a variable acoustic load. 10 15

Regenerator 122 was made from a 7.3 cm stack of 120 mesh stainless steel screen machined to a diameter of 8.89 cm. The stack of screens was contained within a thin wall stainless steel can for ease of installation and removal. Based on the total weight of screen in the regenerator, the volume porosity was 0.72 and the hydraulic radius was about 42 μm . This is smaller than the thermal penetration depth of helium, which varies from 140 μm to 460 μm through regenerator 122. The stainless steel pressure vessel 124 around regenerator 122 had a wall thickness of 12.7 mm at the hot end and was tapered 20 to a thickness of 6.0 mm at the cold end.

Thermal buffer column 126 was an open cylinder having the same inner diameter as regenerator 122 and was 26.4 cm long. Its inner diameter was much larger than the viscous and thermal penetration depths of the helium, and its length was much greater than the gas displacement (2.5 cm) at a typical operating point of $|p_1| / p_m \approx 0.05$. The wall thickness was initially 12.7 mm at the 25 hot end and was stepped down to 6.0 mm at a distance of 9.6 cm from the hot end. No effort was made to taper the thermal buffer column to suppress boundary-layer driven streaming within the column (see U.S. Patent Application 08/975,766). Operating data indicated that this form of streaming was present 30 and was carrying several 100 Watts of heat. These measurements show the need for tapering the thermal buffer column in this type of engine. The small

taper angle θ (a few degrees) shown to reduce streaming in the '766 application would not be readily apparent from Figure 8. Thus, Figure 8 should also be considered to include a tapered embodiment of thermal buffer column 126. It will be appreciated from the '766 application that the amount and direction of the 5 taper that suppresses streaming is not intuitively apparent and must be determined from the particular embodiment and operating conditions of thermal buffer column 126.

For test purposes, hot heat exchanger 128 consisted of an electrically heated Ni-Cr ribbon wound zigzag on an alumina frame. Electrical leads for hot 10 heat exchanger 128 entered thermal buffer column 126 at its ambient temperature end and passed axially up the column to the ribbon. Power flowing into hot heat exchanger 128 was measured using a commercial wattmeter.

First ambient heat exchanger 132 and second ambient heat exchanger 134 were water cooled heat exchangers of shell-and-tube construction. First 15 ambient heat exchanger 132 contained 299 2.5 mm id, 20 mm long tubes. A typical Reynolds number in the tubes was 3,000 at $|p_1| / p_m \approx 0.05$. Second ambient heat exchanger 134 contained 109 4.6 mm id, 10 mm long tubes. A typical Reynolds number in the tubes was 16,000 at $|p_1| / p_m \approx 0.05$. Second ambient heat exchanger 134 was included for test purposes and would not be 20 needed for actual use of the engine.

The main part of inertance 136 was made from commercial, schedule 40, 2.5" nominal, carbon steel pipe. Light machining was performed on the inside surface to improve the finish. To reconnect inertance 136 to the main section of the engine, a standard 2.5" pipe cross 138 and a standard 4" to 2.5" reducing 25 tee 192 were used. The total length of inertance 136 was 59 cm, and the inside diameter was approximately 6.3 cm. Compliance 144 consisted of two commercial, 4" nominal, 90°, short radius elbows. The total volume of compliance 144 was 0.0028 m³. A commercial 4" to 2.5" reducer 146 was used to smoothly adapt inertance 136 to compliance 144. Inertance 136 included 30 sliding joints 148 to allow inertance 136 to lengthen as thermal buffer column 126 and pressure vessel 124 thermally expanded.

In the engine embodiment shown in Figure 8, \dot{M}_2 was suppressed using a hydrodynamic approach, e.g., jet pump 140, discussed below. First, baselines were established for comparison. Engine 120 was run with no attempt made to block \dot{M}_2 . Engine 120 was then operated with rubber diaphragm 152 installed 5 at the junction between reducer 146 and compliance 144. In both of the runs, the pressure phasors p_{10} and p_{1H} were close to the estimates based on prior calculations. The majority of the difference between these two runs is the presence of \dot{M}_2 .

Figure 9 shows the temperature distributions in regenerator 122 in these 10 two runs. In both runs, increasing amounts of heat were applied to hot heat exchanger 128 until the pressure amplitude reached $|p_{10}| / p_m \approx 0.05$. The only load on the engine was the acoustic resonator itself (not shown). Therefore, T_H should be nearly the same for both cases. With the diaphragm in place, the 15 temperature rises linearly from the ambient end to the hot end. With no \dot{M}_2 , this linear dependence is expected because the thermal conductivity of helium and stainless steel depend only weakly on temperature.

The temperature distribution with diaphragm 152 removed and \dot{M}_2 not restricted is greatly different. Equation 9 and the subsequent discussion show that \dot{M}_2 flows in the same direction as the flow of acoustic power. In this case 20 \dot{M}_2 enters regenerator 122 from first ambient heat exchanger 132. As seen in Figure 9, this flux of cold gas reduces the temperature of regenerator 122 for nearly its entire length. The temperature rises quickly near the hot end due to the presence of hot heat exchanger 128. Note that, in Figure 9, the lines are only guides to the eye, and do not reflect the actual temperatures between the 25 data points. The temperature near 7.2 cm can be assumed to be nearly the same as that at 10 cm. For a rough estimate of \dot{M}_2 , compare the amounts of heat input, \dot{Q}_H , needed to run the engine at this pressure amplitude with and without diaphragm 152. With diaphragm 152 in place, $\dot{Q}_H = 1250$ W. Without

diaphragm 152, $\dot{Q}_H = 2660$ W. This difference in heat input, $\Delta\dot{Q}_H$, should be given by

$$\Delta\dot{Q}_H = \dot{M}_2 c_p (T_H - T_0) \quad (14)$$

Using Equation (14), $\dot{M}_2 \approx 1.5 \times 10^{-3}$ kg/s.

One way to suppress \dot{M}_2 is to impose a time averaged pressure drop,

5 Δp_2 across regenerator 122 that would drive an equal but oppositely directed amount of \dot{M}_2 through regenerator 122. The required Δp_2 can be estimated using the low-Reynolds-number limit of Figure 7-9 of Kays and London, Compact Heat Exchangers, (McGraw-Hill, NY 1964), incorporated herein by reference,

$$\frac{dp_2}{dx} \approx -\frac{6\dot{M}_2\mu}{\rho_m S r_h^2} \quad (15)$$

10 for the pressure gradient in a screen bed of cross-sectional area S and hydraulic radius r_h , where μ is the viscosity. The numerical factor depends weakly on the volumetric porosity of the bed. For the data shown in Figure 9 and the estimate of \dot{M}_2 , the required pressure drop is 370 Pa.

An alternate way to estimate \dot{M}_2 within regenerator 122 is to use Equation (9) and the subsequent discussion, i.e., $\dot{M}_2 = \rho_m \dot{W}_2 / p_m$. Under the 15 conditions of the experiment, at the ambient end of regenerator 122, \dot{W}_2 is calculated to be $\dot{W}_2 = 850$ W giving $\dot{M}_2 = 1.3 \times 10^{-3}$ kg/s. The experimental estimate of \dot{M}_2 and the calculation are in rough agreement, suggesting that the estimate of $\Delta p_2 \sim 370$ Pa is approximately correct.

In the limit of low viscosity or large tube diameters and in the absence of 20 turbulence, p_2 would be described by some acoustic version of the Bernoulli equation. This suggests that an acoustically ideal path connecting the two ends of the regenerator would impose across regenerator 122 a pressure difference of the order of $\Delta[\rho_m u_1 \tilde{u}_1]$ where u_1 is the complex velocity amplitude. (Such an ideal path might include a thermal buffer column, inertance, and compliance, 25 without heat exchangers or other components having small passages.) This

pressure difference is typically much smaller than the Δp_2 that is required for $\dot{M}_2 = 0$. Hence, to produce the required Δp_2 an additional physical effect or structure in the path is needed, relying on turbulence, viscosity, or some other physical phenomenon not included in the Bernoulli equation.

5 Asymmetry in hydrodynamic end effects can produce this required Δp_2 . In a tapered transition between a small-diameter tube, where $|u_1|$ is large, and a large-diameter tube, where $|u_1|$ is small, turbulence would be avoided and Bernoulli's equation would hold if the taper were sufficiently gentle. At the opposite extreme, for an abrupt transition, a large $|u_1|$ generates significant
 10 turbulence, and further the oscillatory pressure drop across an abrupt transition should reflect the phenomena known as "minor losses" in high-Reynolds-number steady flow. If the gas displacement amplitude is much greater than the tube diameter, the flow at any instant of time has little memory of its past history, so that the acoustic behavior can be deduced from careful time integration of the
 15 well-known expressions for the steady-flow phenomena.

In steady flow through an abrupt transition, the minor loss-induced deviation Δp_{ml} of the pressure from the Bernoulli equation ideal is given by

$$\Delta p_{ml} = K \frac{1}{2} \rho u^2 \quad (16)$$

where K is the minor-loss coefficient, which is well known for many transition geometries, and u is the velocity. K depends strongly on the direction of flow
 20 through the transition. In the example shown in Figures 10A and 10B, a small flanged tube 160 is connected to an essentially infinite open space 164. When a gas 164 (at velocity u inside tube 162) flows out of the tube 162, a jet occurs, and kinetic energy is lost to turbulence 166 downstream of the jet; $K_{out} = 1$. In contrast, when gas flows into tube 162, as shown in Figure 10B, streamlines 168
 25 in open space 164 are widely and smoothly dispersed; K_{in} is between 0.5 and 0.04, with smaller values for larger radius r of rounding of the edge of the entrance.

If $u_1 = |u_1| \sin \omega t$, the time-averaged pressure drop is obtained by integrating Equation (16) in time:

$$\overline{\Delta p_{ml}} = \frac{\omega}{2\pi} \left(\int_0^{\pi/\omega} K_{out} \frac{1}{2} \rho |u_1|^2 \sin^2 \omega t dt - \int_{\pi/\omega}^{2\pi/\omega} K_{in} \frac{1}{2} \rho |u_1|^2 \sin^2 \omega t dt \right) \\ = \frac{1}{8} \rho |u_1|^2 (K_{out} - K_{in}) \quad (17)$$

This hydrodynamic mean pressure difference can be used as the source of Δp_2 across the regenerator necessary to force $\dot{M}_2 = 0$. Such simple control of \dot{M}_2 is

5 not without penalty, however; acoustic power is dissipated at a rate

$$\dot{E} = S \frac{\omega}{2\pi} \int_0^{2\pi/\omega} \Delta p_{ml} u dt \\ = S \frac{\omega}{2\pi} \left(\int_0^{\pi/\omega} K_{out} \frac{1}{2} \rho |u_1|^3 \sin \omega t dt - \int_{\pi/\omega}^{2\pi/\omega} K_{in} \frac{1}{2} \rho |u_1|^3 \sin^3 \omega t dt \right) \\ = \frac{1}{3\pi} \rho |u_1|^2 |U_1| (K_{out} + K_{in}) \quad (18) \\ = \frac{8}{3\pi} \overline{\Delta p_{ml}} |U_1| \frac{K_{out} + K_{in}}{K_{out} - K_{in}} \quad (19)$$

where S is the area of the small tube 162. Equation (19) shows that the best way to produce a desired $\overline{\Delta p_{ml}}$ is to insert the hydrodynamic mass-flux suppressor at a location where $|U_1|$ is small, and to shape it so that $K_{out} - K_{in}$ is as large as possible.

10 In engine 120 (Figure 8), $|U_1|$ is smallest adjacent to regenerator 122, but that was an inconvenient location for adding an additional component. Second ambient-temperature heat exchanger 134 has only slightly larger $|U_1|$ and already requires some extra dissipation to ensure that p_{10} leads p_{1H} slightly, so the space below second ambient temperature heat exchanger 134 was chosen
15 as the location for experiments on hydrodynamic mass-flux suppression. In this embodiment, hydrodynamic mass-flux suppressor 140 was a "jet pump", formed from a brass block bored through with 25 identical tapered holes, each 1.82 cm long, 8.05 mm diameter at the upper end nearest second ambient temperature

heat exchanger 134, and 5.72 mm diameter at the lower end. End effects at the well-rounded small ends of the holes are strongly asymmetric, causing the desired Δp_{ml} , while the velocities at the large ends of the holes are small enough that minor losses are negligible. The tapers joining the ends are gradual enough
5 to prevent minor losses in-between. For the chosen geometry, jet pump 140 was estimated to create a pressure of $\Delta p_2 = 930$ Pa. However, this estimate is based on a calculation that assumes no interaction between the minor losses at the two ends of jet pump 140. For steady flow, it is known that two minor loss sites located close together result in less Δp_2 than the sum of the individual
10 Δp_2 's.

Jet pump 140 was installed and engine 120 was run at the same operating point as the two other sets of data in Figure 9. The temperature distribution with jet pump 140 was nearly restored to the distribution with rubber diaphragm 152. Also, the amount of heat input needed to reach this operating
15 point with rubber diaphragm 152 was only $\dot{Q}_H = 1520$ W. The additional heat required without the rubber diaphragm 152 was 1400 Watts. The use of jet pump 140 reduced this by 82% to 260 Watts. This clearly demonstrates the effectiveness of jet pump 140.

By using a variable acoustic load (not shown) to increase the acoustic
20 load on the engine, measurements of the temperature distribution were made as a function of T_H at a fixed value of $|p_{10}| / p_m = 0.05$. These measurements showed no detectable change in the linearity of the temperature distribution for $200^\circ \leq T_H \leq 725^\circ\text{C}$. Therefore, jet pump 140 appeared to be very immune to variations in the load conditions. Finally, by varying \dot{Q}_H at fixed acoustic load,
25 measurements were made of the temperature distribution as function of p_1 at fixed $T_H \approx 525^\circ\text{C}$. The temperature distribution did not change in the range $0.03 \leq |p_{10}| / p_m \leq 0.05$. At higher pressure amplitudes, the jet pump weakened relative to other sources of Δp_2 . At the highest pressure amplitude achieved, $|p_{10}| / p_m = 0.075$, the temperature in the middle of the regenerator dropped from

its low amplitude value of 310°C to 235°C. This amounts to only a 15% change relative to $T_H - T_0 \approx 500^\circ\text{C}$.

The efficiencies obtained during these measurements with jet pump 140 are shown in Figures 11A and 11B. During these measurements, the highest efficiency $\eta = \dot{W}/Q_H = 0.17$, and the highest fraction of Carnot efficiency, $\eta_{II} = \eta/\eta_C = 0.27$, where the Carnot efficiency is $\eta_C = 1 - T_0/T_H$. With rubber diaphragm 152 in place, the highest observed values were $\eta = 0.21$ and $\eta_{II} = 0.32$. In measuring the work output of the engine, \dot{W} , only the acoustic power delivered to the variable acoustic load was counted; the resonator dissipation was not included. Hence, these efficiencies represent the engine plus resonator; the efficiencies with which the engine delivered power to the resonator are even higher.

It may sometimes be desirable to adjust the strength of the hydrodynamic method for mass-flux suppression while a traveling-wave device is operating in order to provide whatever Δp_2 is needed to enforce $\dot{M}_2 = 0$ over a broad range of operating conditions. To test such a variable hydrodynamic method, the refrigerator apparatus shown in Figure 6 was modified to include a slit jet pump as shown in Figures 12A and 12B in place of flexible diaphragm 108 shown in Figure 6. Slit 172 provides asymmetric flow as illustrated in Figures 10A and 10B, and hence provides Δp_2 as shown in Equation (17) with $K_{out} \sim 1$ and $K_{in} \sim 0.1$. Pivot point 174 allows right wall 176 of slit 172 to be moved, e.g., by a lever (not shown) connected through a pressure seal to an external knob for manual adjustment or by an automatic controller that is regulated by, e.g., a temperature sensor in the middle of regenerator 98 (Figure 6). Moving right wall 176 of slit 172 in this way adjusted the area of slit 172, and hence changed $|u_1|$ relative to $|U_1|$ so that Δp_2 was changed according to Equation (17).

Tests with this setup over a range of T_C (from 0° to -70°C) and a range of pressure amplitudes $|p_1|/p_m$ (from 0.03 to 0.05) showed that the width of slit 172 could be adjusted to keep the temperature in the middle of regenerator 98

approximately equal to the average of T_C and T_0 , indicative of $\dot{M}_2=0$. Under these circumstances, the performance of the refrigerator was similar to its performance when flexible diaphragm 108 was used.

The above description of the invention is mostly in terms of a refrigerator with a sub-wavelength torus and with a flexible-barrier method of mass-flux suppression and in terms of an engine with a sub-wavelength torus and with a hydrodynamic method of mass-flux suppression. However, the use of a thermal buffer column and either method of mass-flux suppression is applicable to both engines and refrigerators, whether these engines and refrigerators employ sub-wavelength tori as described herein or more nearly full-wavelength tori as described by Ceperley. It should also be apparent from the description that additional flexible-barrier methods (including bellows) and additional hydrodynamic methods (including the adjustable method discussed above) are also useful. Although mass-flux suppression is described herein as localized, it could be distributed throughout several regions of the apparatus, such as by employing tapered passages in one or more heat exchangers and using asymmetric hydrodynamic effects at the "tee" joining the torus and the side branch (see, e.g., Figure 8).

It should also be apparent that all aspects of the present invention are as applicable to heat pumps as to refrigerators, that an engine and refrigerator can share the same torus, that multiple devices can share a torus, and that multiple tori can be connected in many ways, such as by sharing a common inertance and a common compliance. In such situations, each torus may require its own mass-flux suppressor, and each heat exchanger at a temperature other than ambient temperature may benefit from an adjacent thermal buffer column.

Figures 13A-D illustrate some of these embodiments. In the description of these figures, the terms regenerator, heat exchanger, mass-flux suppressor, thermal buffer, inertance, compliance, and other terms have the same meaning as with the above detailed descriptions and will not be described in detail. It is the arrangement of these components that provides the different embodiments and not the function of the components.

Referring first to Figure 13A, there is shown a heat pump configuration of components. Torus 180 defines inertance 202 and compliance 198. Regenerator 182 is located in torus 180 with an ambient heat exchanger 184 downstream from regenerator 182 relative to the circulating acoustic power. Hot 5 heat exchanger 186 is adjacent to and upstream of regenerator 182. Mass flux suppressor 185 is shown downstream from ambient heat exchanger 184, but may be located at any convenient location in torus 180. In this instance, thermal buffer column 188 is located adjacent hot heat exchanger 186, which is the heat exchanger that defines the operating temperature of the device. Acoustic power 10 192 is generated by acoustic device 196 and input to torus 180 through side branch 194.

Figure 13B depicts a combination of an acoustic source 40 formed by an engine according to the present invention as described in Figure 4 and an acoustic sink 76 formed by a refrigerator according to the present invention as 15 described in Figure 3, where like numbers represent like components that can be identified by reference to Figures 3 and 4. A common side branch corresponds to side branches 44 and 74 with acoustic power flow 42, 72 as shown in Figures 3 and 4.

Figure 13C is a further refinement of the embodiment shown in Figure 20 13B where engine 212 and refrigerator 230 are incorporated into a single torus 210. Engine 212 includes regenerator 216, with adjacent heat exchangers 214 (ambient temperature) and 218 (operating temperature), with operating temperature heat exchanger 218 downstream from regenerator 216 and adjacent thermal buffer column 222 downstream from operating temperature 25 heat exchanger 218. If needed, engine 212 may have associated inertance 224 and compliance 226 to provide suitable phasing of the output acoustic power.

Refrigerator 230 receives the acoustic power output from engine 212 and includes regenerator 234 with adjacent heat exchangers 232 (ambient temperature) and 236 (operating temperature). Thermal buffer column 238 is 30 downstream from operating temperature heat exchanger 236. If needed, additional inertance 242 and compliance 244 may be defined by torus 210. In accordance with the present invention, mass-flux suppressor 240 is included in

torus 210. Suppressor 240 may be generally located anywhere within torus 210 and may be lumped at one location or provided as a distributed suppressor or discrete multiple components within torus 210.

Figure 13D schematically depicts a parallel configuration of multiples of the refrigerator shown in Figure 3. Identical components are described with the same reference numbers or primed reference numbers and are individually discussed with reference to Figure 3. As shown, one or more refrigerator sections may be joined by a common column 50 for the circulating acoustic power 38, 38'. Column 50 may be configured to define a common inertance for the parallel refrigerators. It will be understood that more than two refrigerators may be connected in parallel. Also, while Figure 13D depicts refrigerators, the same configuration could be used for the engine shown in Figure 4.

The foregoing description of Stirling cycle traveling-wave refrigerators and engines has been presented for purposes of illustration and description and is not intended to be exhaustive or to limit the invention to the precise form disclosed, and obviously many modifications and variations are possible in light of the above teaching. The embodiments were chosen and described in order to best explain the principles of the invention and its practical application to thereby enable others skilled in the art to best utilize the invention in various embodiments and with various modifications as are suited to the particular use contemplated. It is intended that the scope of the invention be defined by the claims appended hereto.

WHAT IS CLAIMED IS:

1. A pistonless traveling-wave device having
 - a. a torus for circulating acoustic energy in a direction through a fluid;
 - b. a regenerator located in the torus;
 - c. a first heat exchanger located on a downstream side of the regenerator relative to the direction of the circulating acoustic energy; and
 - d. a second heat exchanger located on an upstream side of the regenerator;
- wherein the improvement comprises:
 - e. a mass-flux suppressor located in the torus to minimize time averaged mass flux of the fluid.
2. A pistonless traveling-wave device according to Claim 1, further including:
 - f. a thermal buffer column located in the torus adjacent the one of the first or second heat exchangers that is at an operating temperature of the traveling-wave device to thermally isolate that heat exchanger.
3. A pistonless traveling-wave device according to either one of Claims 1 or 2, wherein the torus is shorter than a wavelength of the circulating acoustic energy.
4. A pistonless traveling-wave device according to Claim 3, wherein the torus defines acoustic inertance and acoustic compliance portions.
5. A pistonless traveling-wave device according to Claim 2, wherein the thermal buffer column has a diameter much greater than a viscous penetration depth of the fluid.
6. A pistonless traveling-wave device according to Claim 2, wherein the thermal buffer column has a length greater than a peak-to-peak fluid displacement amplitude.
7. A pistonless traveling-wave device according to any one of Claims 5 or 6, wherein the thermal buffer column is tapered.

8. A pistonless traveling-wave device according to any one of Claims 1 or 2, wherein the mass-flux suppressor is a flexible diaphragm.

9. A pistonless traveling-wave device according to any one of Claims 1 or 2, wherein the mass-flux suppressor is a hydrodynamic jet pump having a geometry effective to provide asymmetric end effects to generate a pressure drop to oppose mass flux through the jet pump.

10. A pistonless traveling-wave device according to any one of Claims 1 or 2, wherein the device is a refrigerator and the downstream heat exchanger is a cold heat exchanger.

11. A pistonless traveling-wave device according to Claim 10, wherein the torus is shorter than a wavelength of the circulating acoustic energy.

12. A pistonless traveling-wave device according to Claim 11, where the torus defines acoustic inertance and acoustic compliance portions.

13. A pistonless traveling-wave device according to any one of Claims 1 or 2, wherein the device is an engine and the downstream heat exchanger is a hot heat exchanger.

14. A pistonless traveling-wave device according to Claim 13, wherein the torus is shorter than a wavelength of the circulating acoustic energy.

15. A pistonless traveling-wave device according to Claim 14, wherein the torus defines acoustic inertance and acoustic compliance portions.

16. A pistonless traveling-wave device according to any one of Claims 1 or 2, wherein the device is a heat pump and the upstream heat exchanger is a hot heat exchanger.

17. A pistonless traveling-wave device according to Claim 16, wherein the torus is shorter than a wavelength of the circulating acoustic energy.

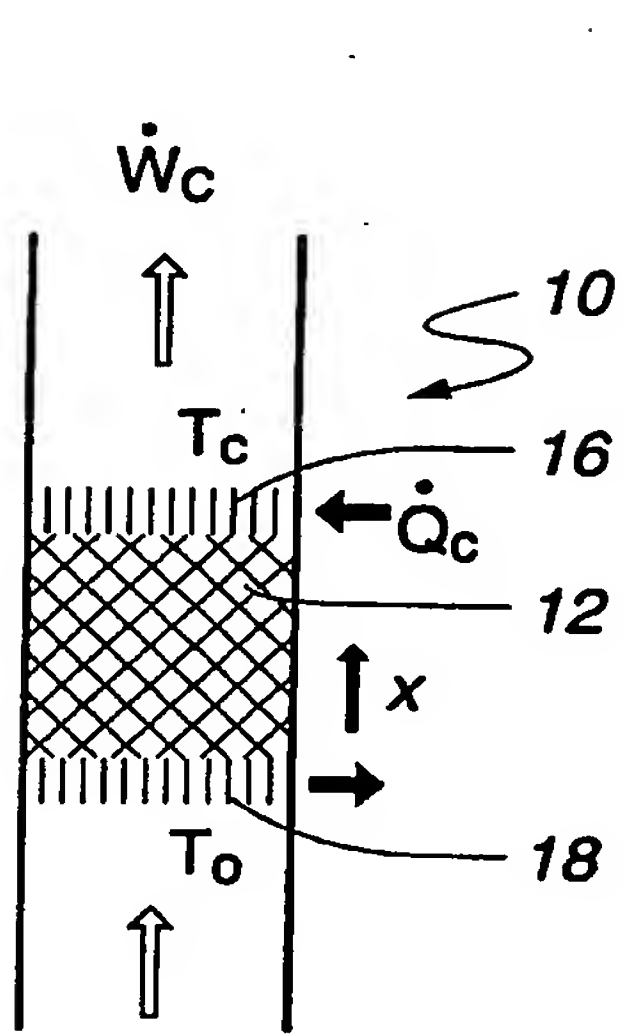
18. A pistonless traveling-wave device according to Claim 17, wherein the torus defines acoustic inertance and acoustic compliance portions.

19. A pistonless traveling-wave device according to Claim 10, further including an engine for generating the acoustic energy having a second regenerator, a hot heat exchanger downstream of the second regenerator relative to a direction for propagating the acoustic energy and an ambient heat exchanger upstream of the second regenerator.

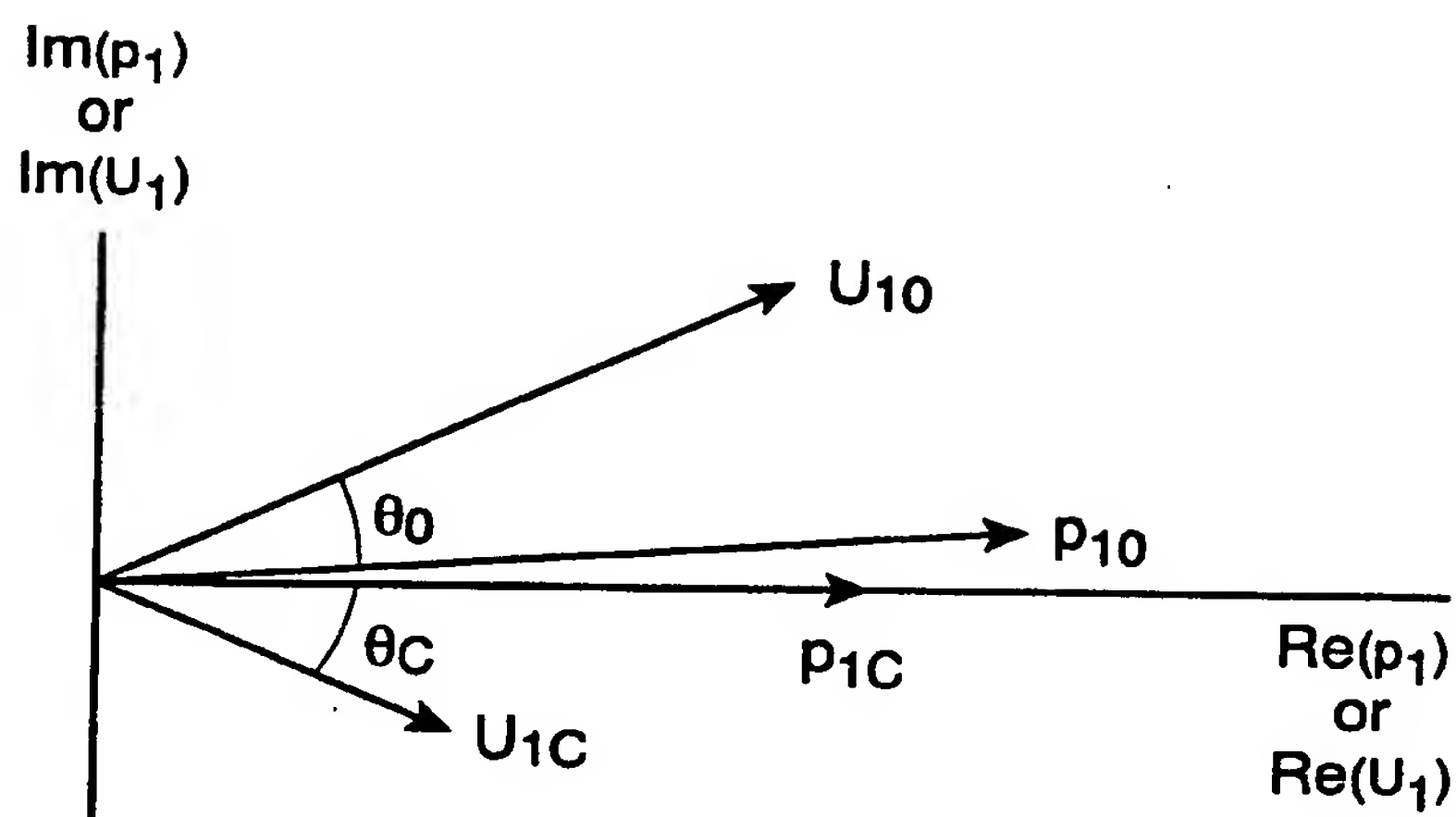
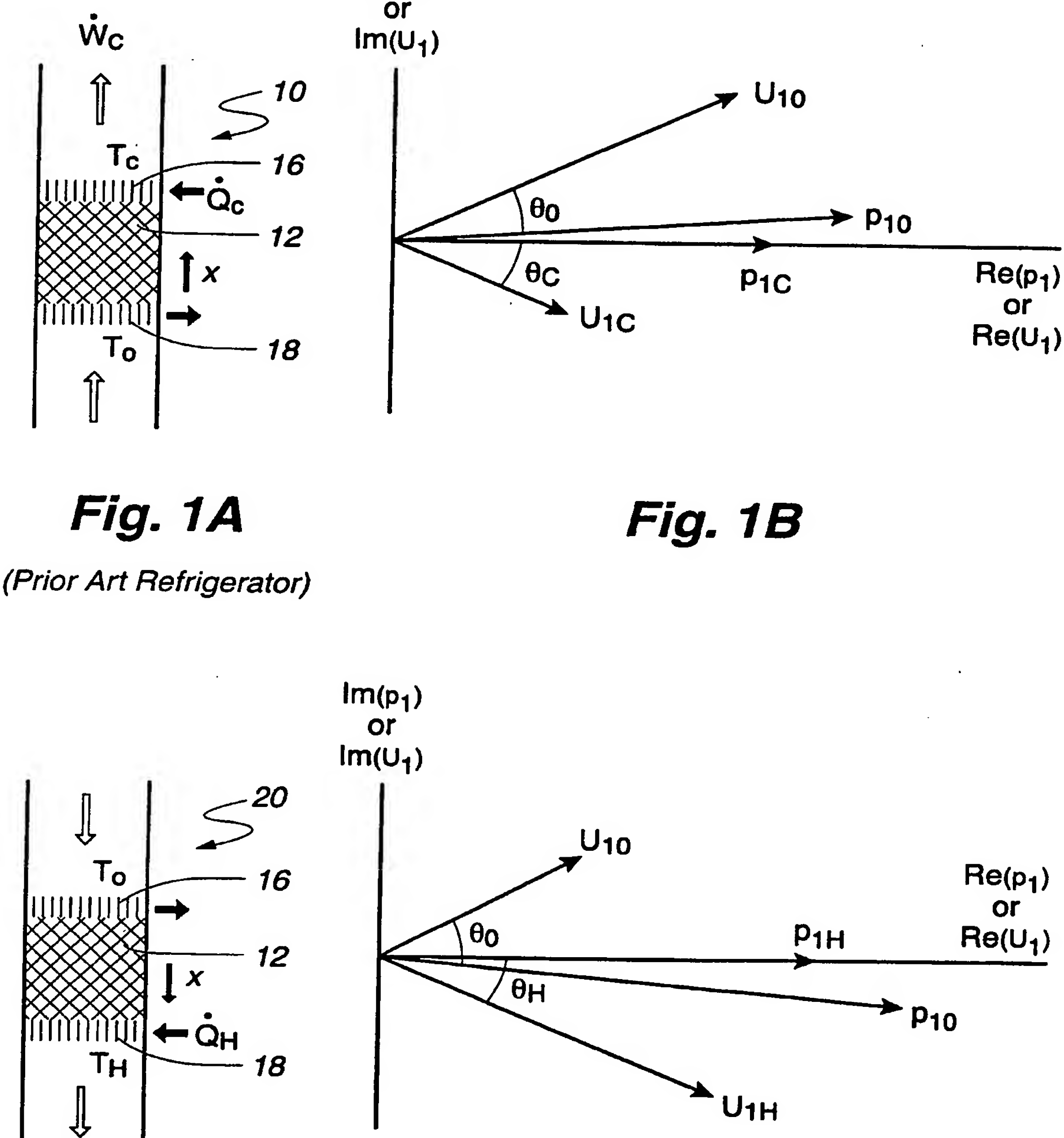
5 20. A pistonless traveling-wave device according to Claim 19, wherein the engine is located in a second torus connected to the torus with the refrigerator and the second torus includes a second mass-flux suppressor.

21. A pistonless traveling-wave device according to Claim 19, wherein the engine is located in the torus with the refrigerator.

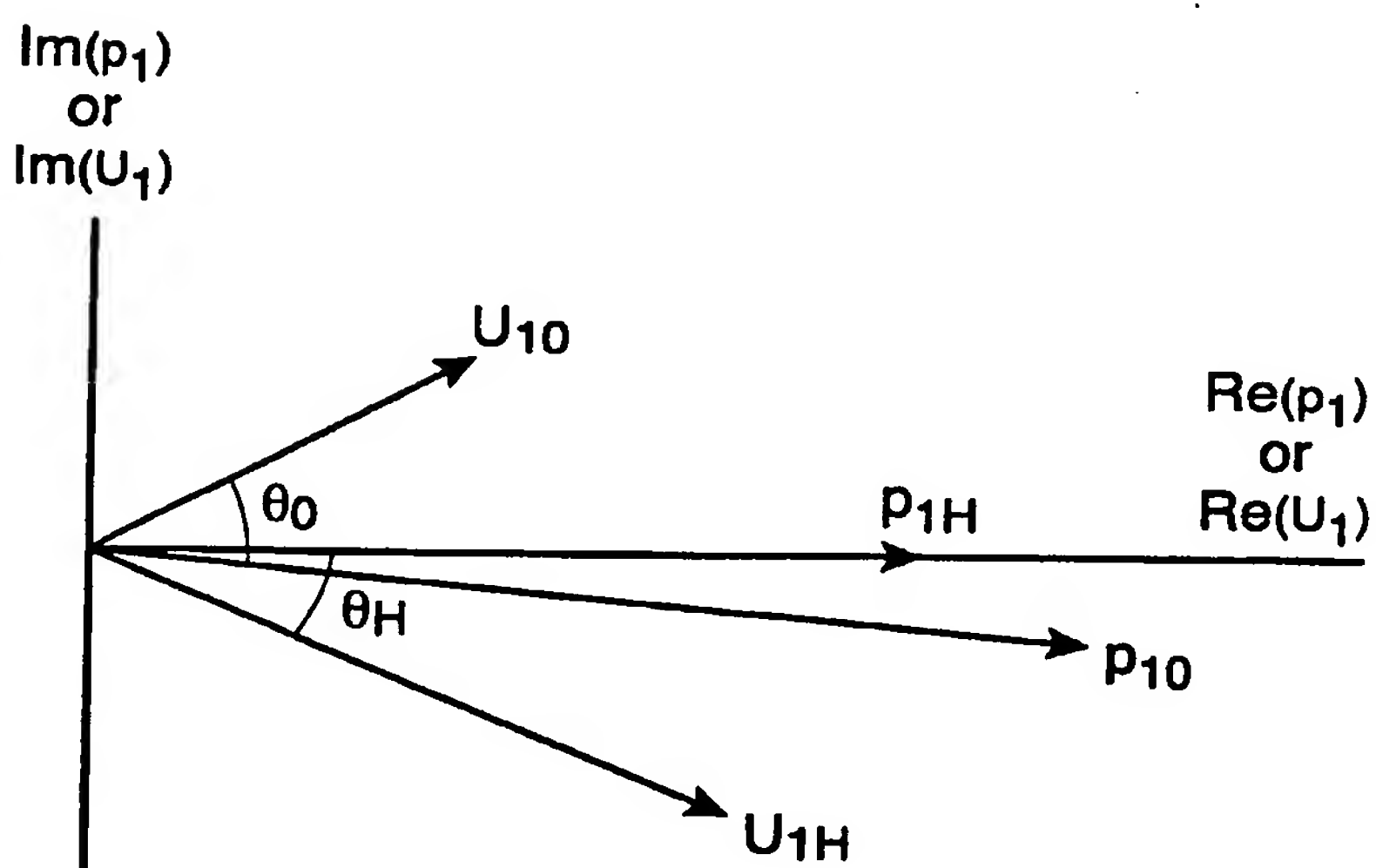
22. A pistonless traveling-wave device according to Claim 10, further including at least a second refrigerator in a second torus, where the second torus has at least a portion of the volume in common with the torus to form a parallel connection of the refrigerator and the second refrigerator.

**Fig. 1A**

(Prior Art Refrigerator)

**Fig. 1B****Fig. 2A**

(Prior Art Engine)

**Fig. 2B**

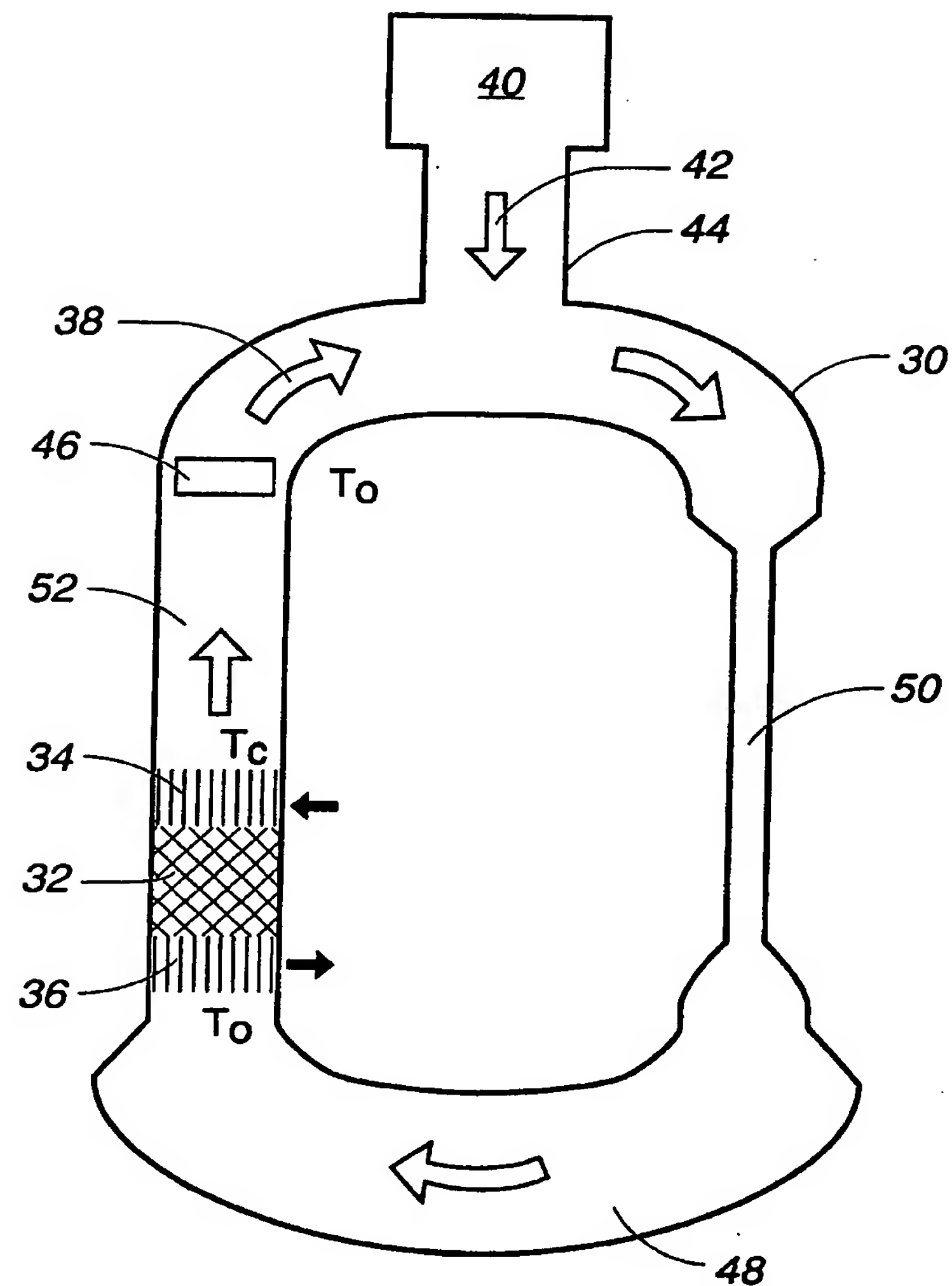


Fig. 3

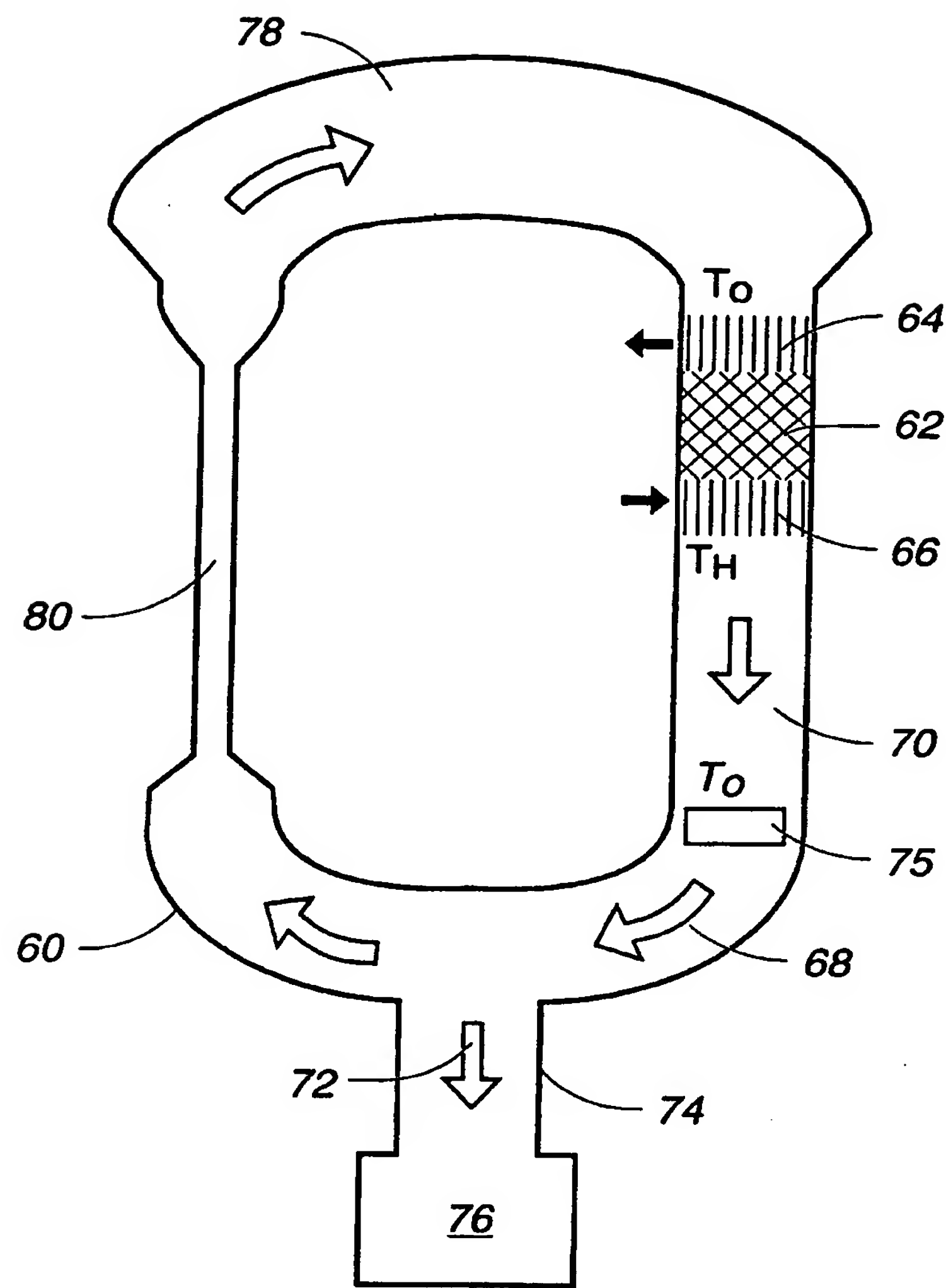


Fig. 4

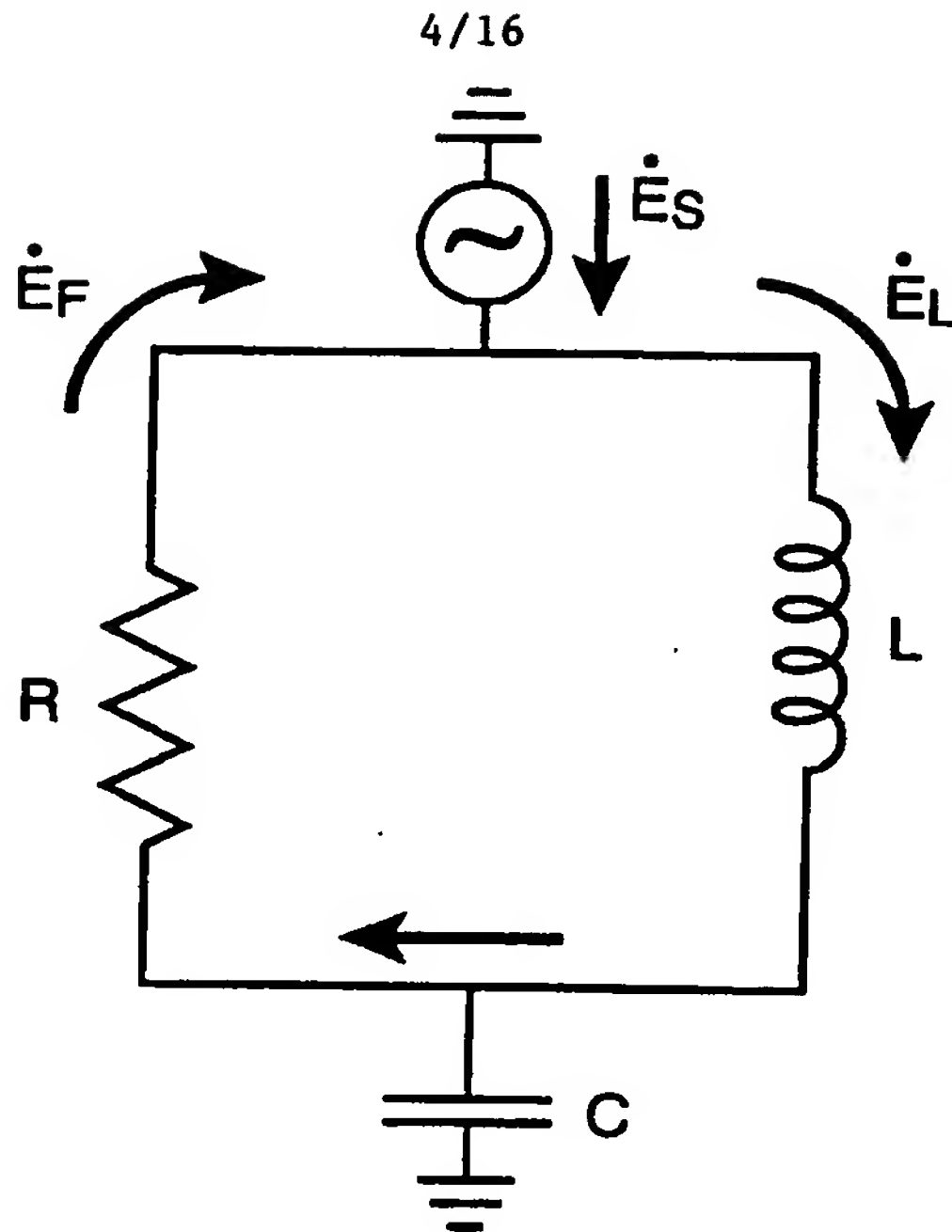


Fig. 5A

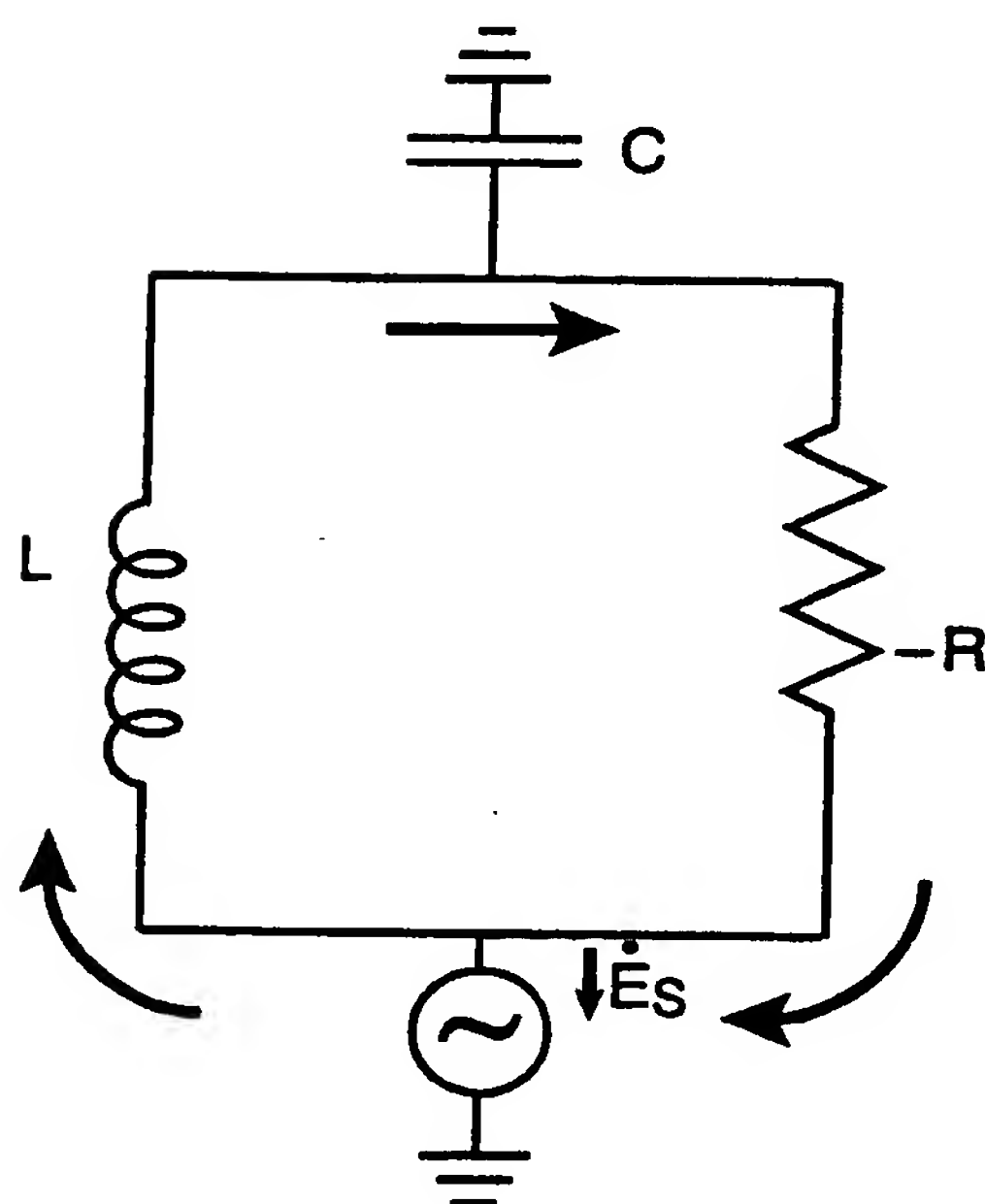


Fig. 5B

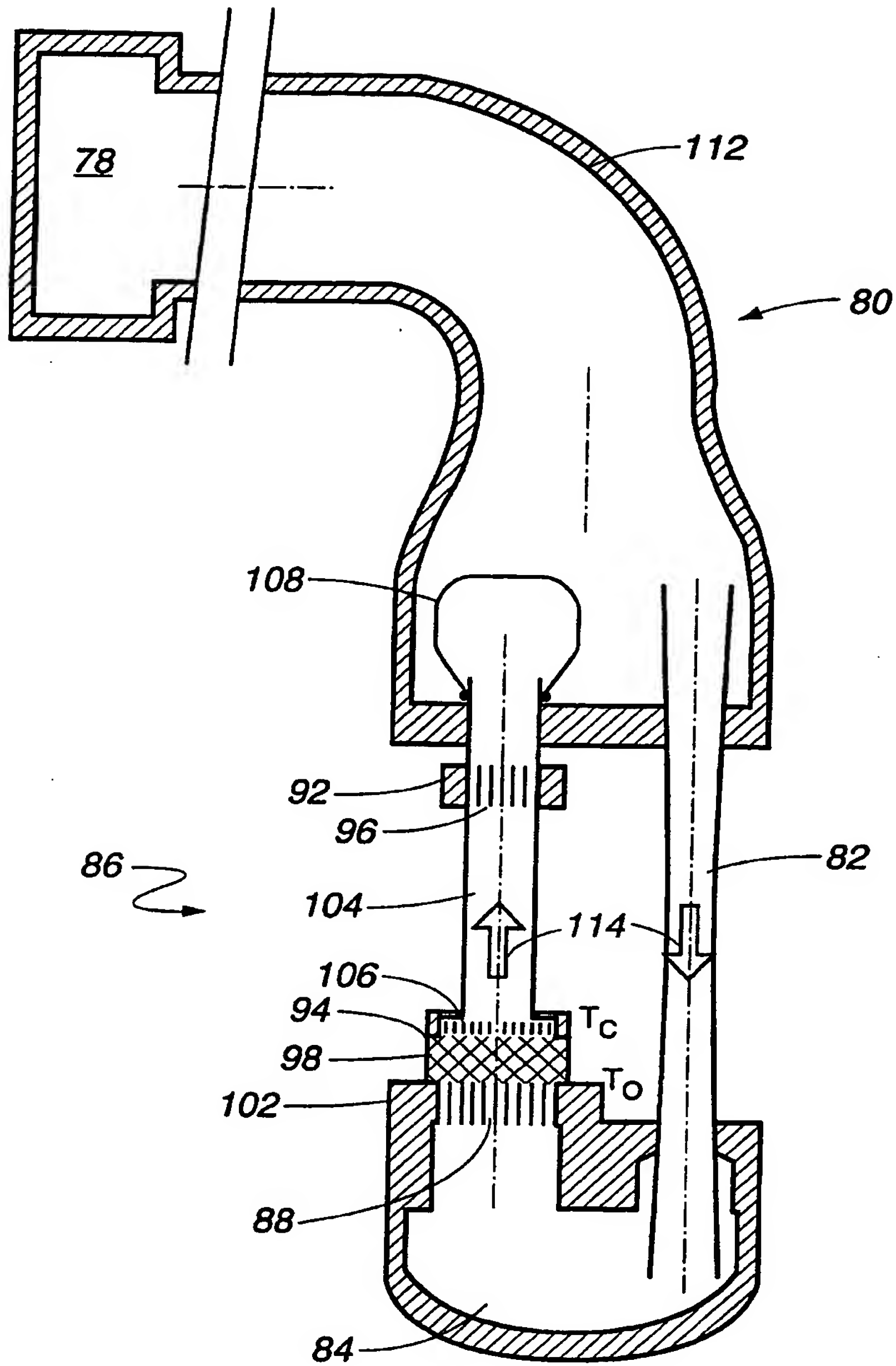


Fig. 6

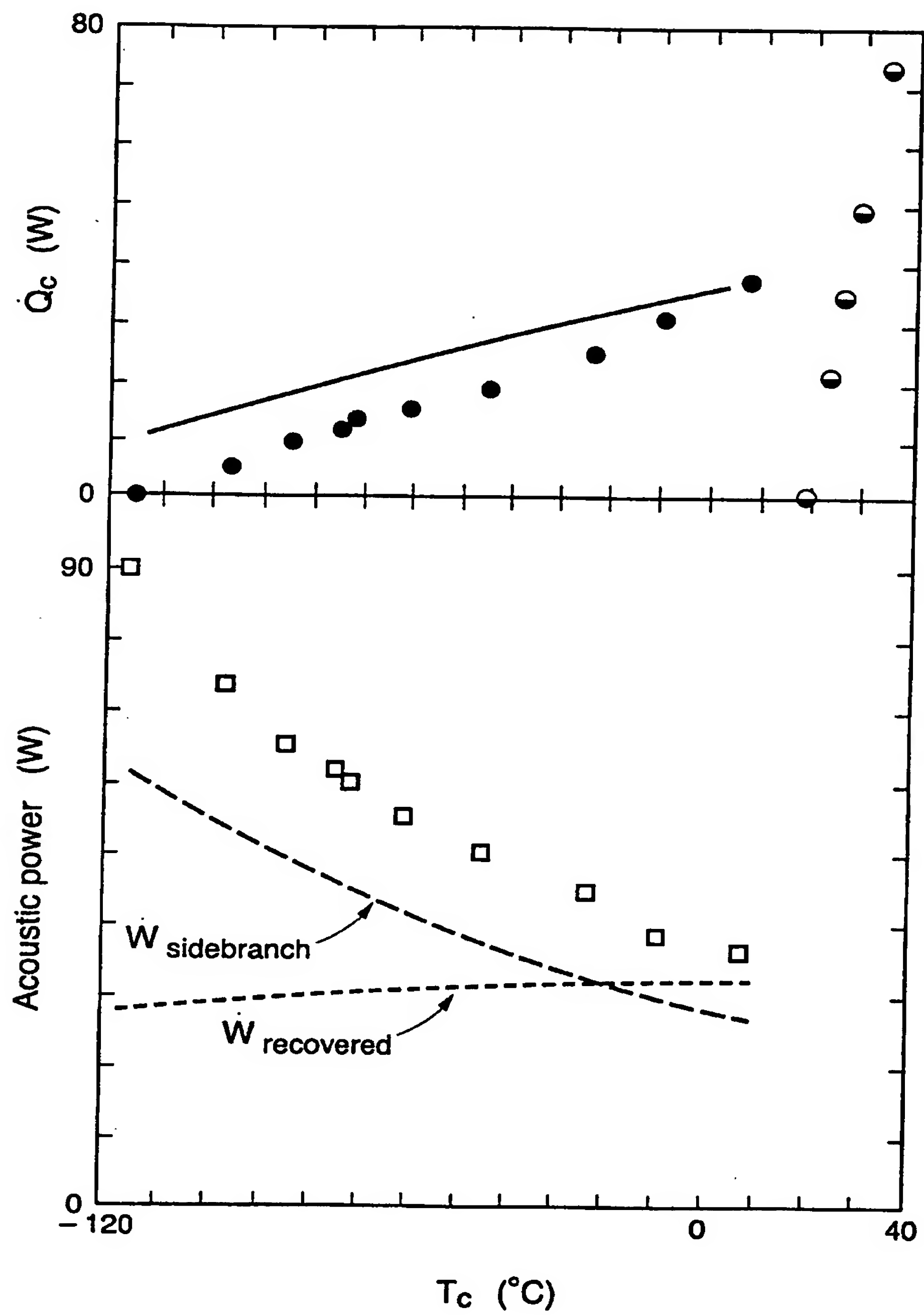


Fig. 7

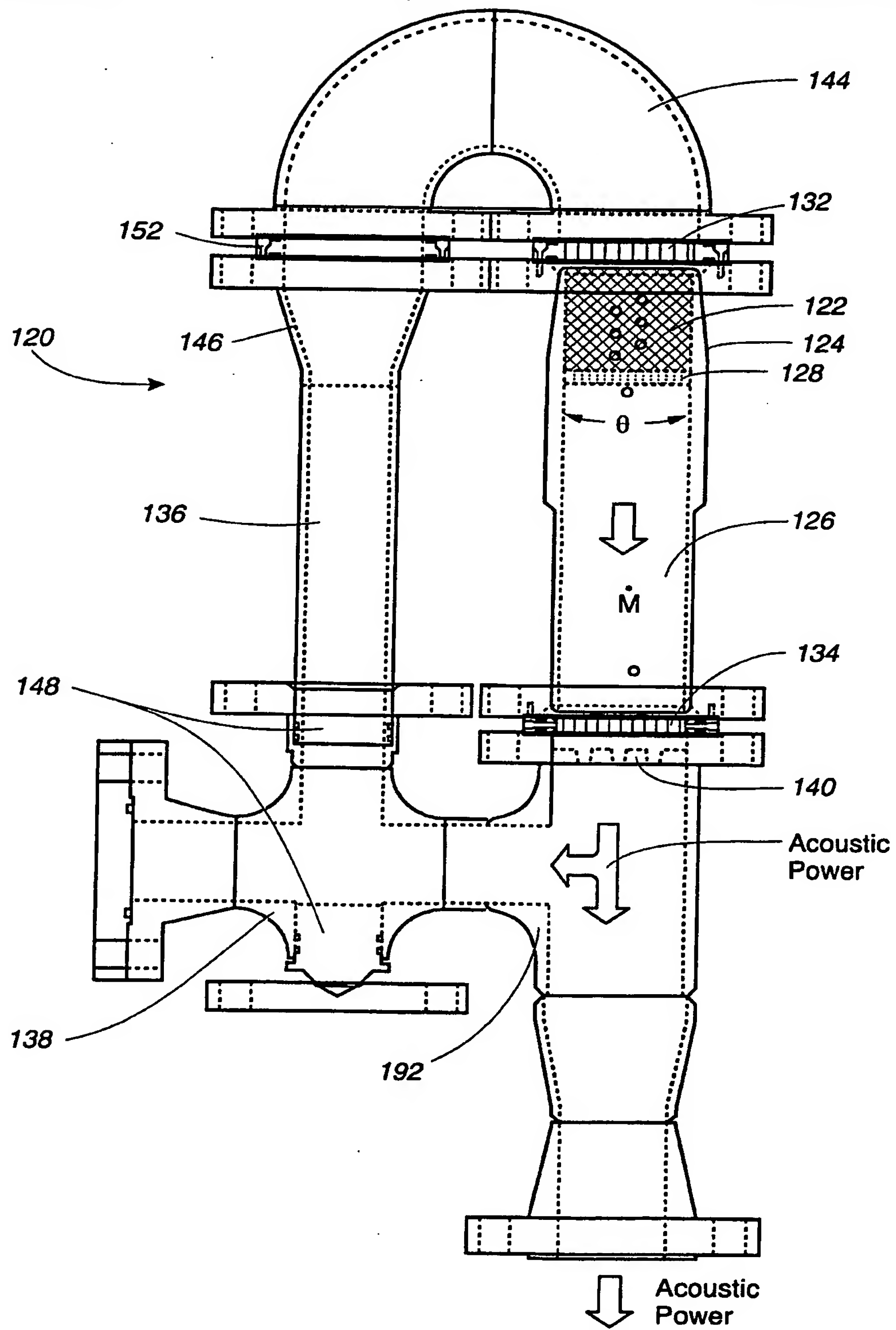


Fig. 8

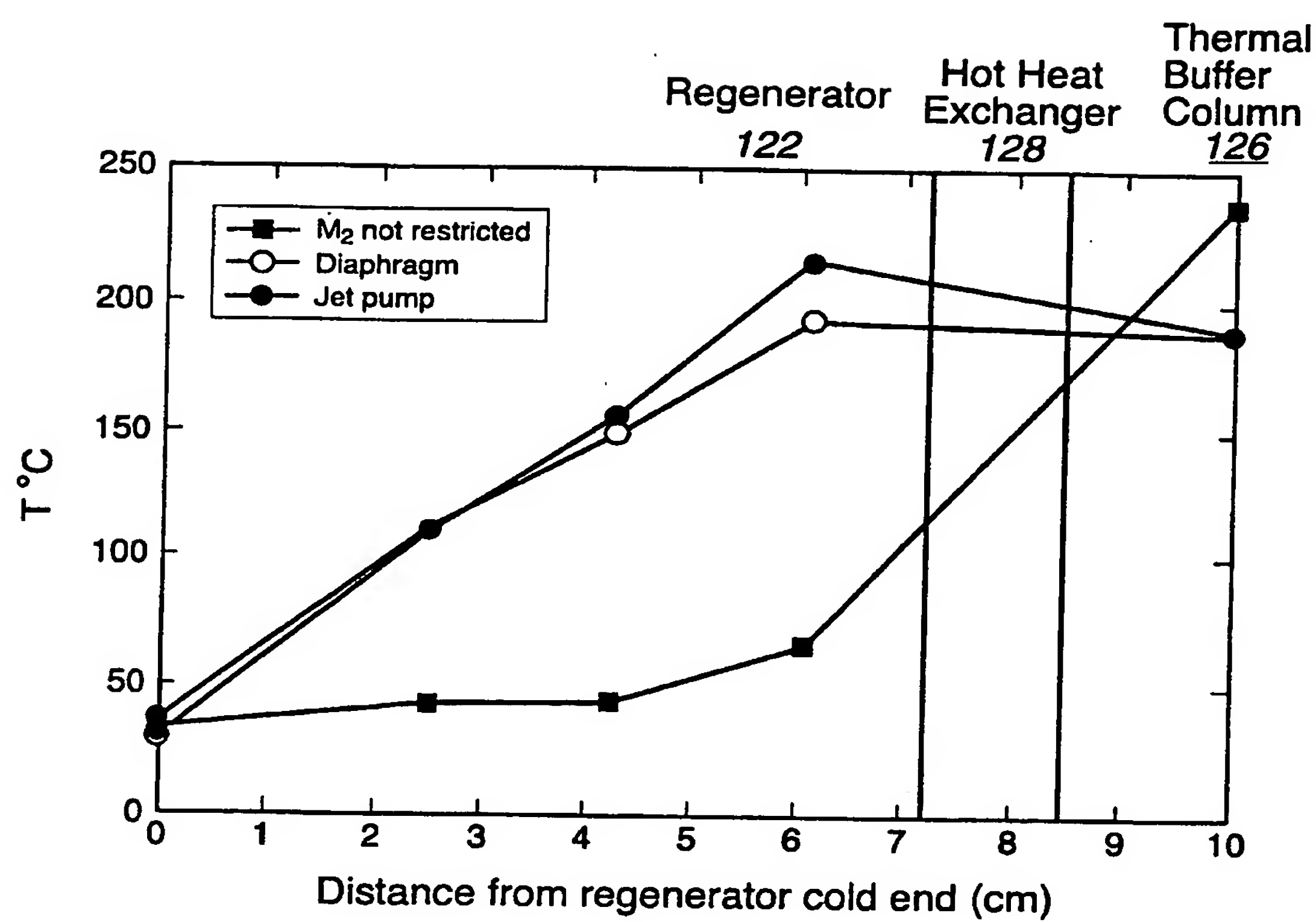


Fig. 9

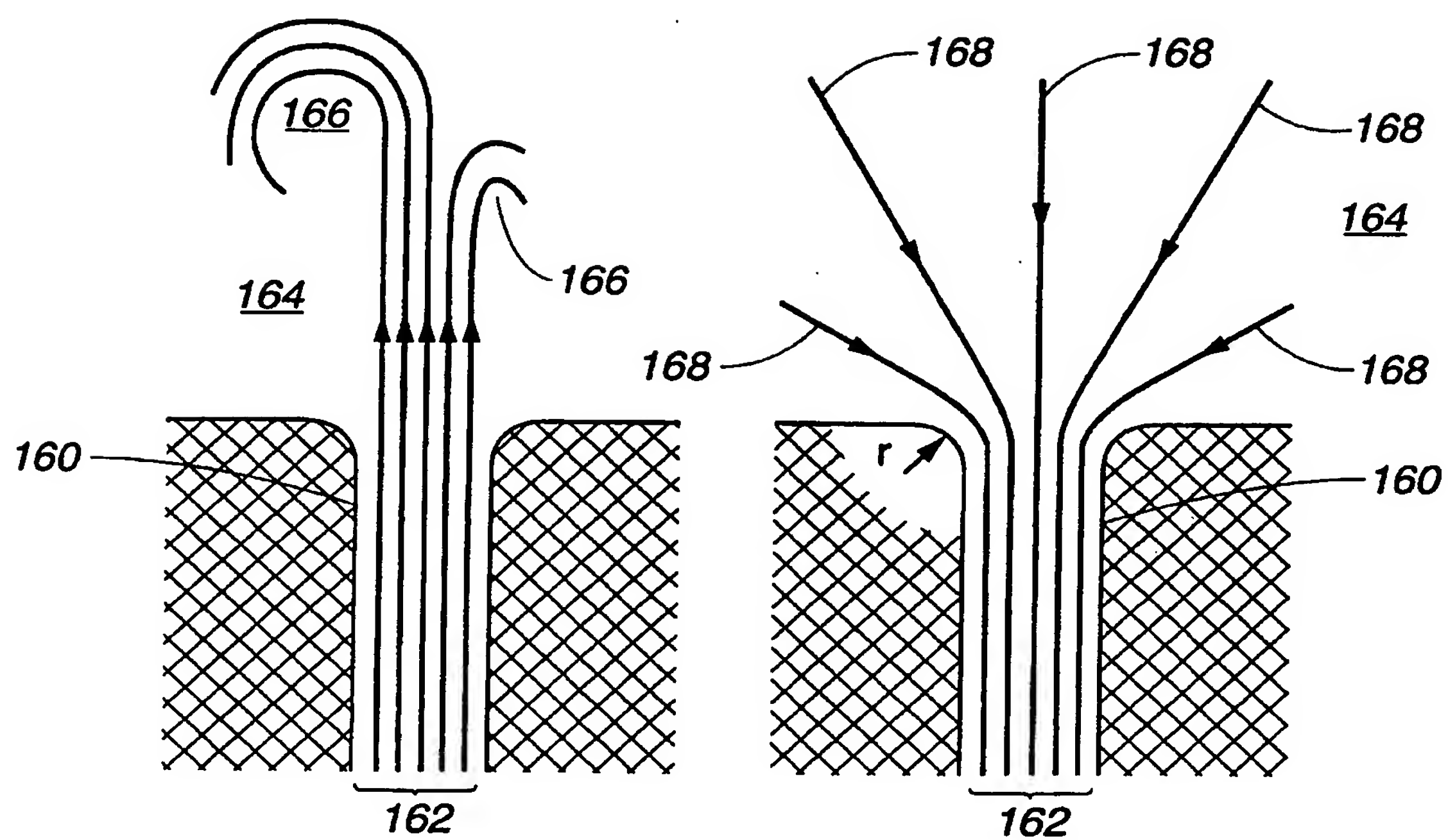


Fig. 10A

Fig. 10B

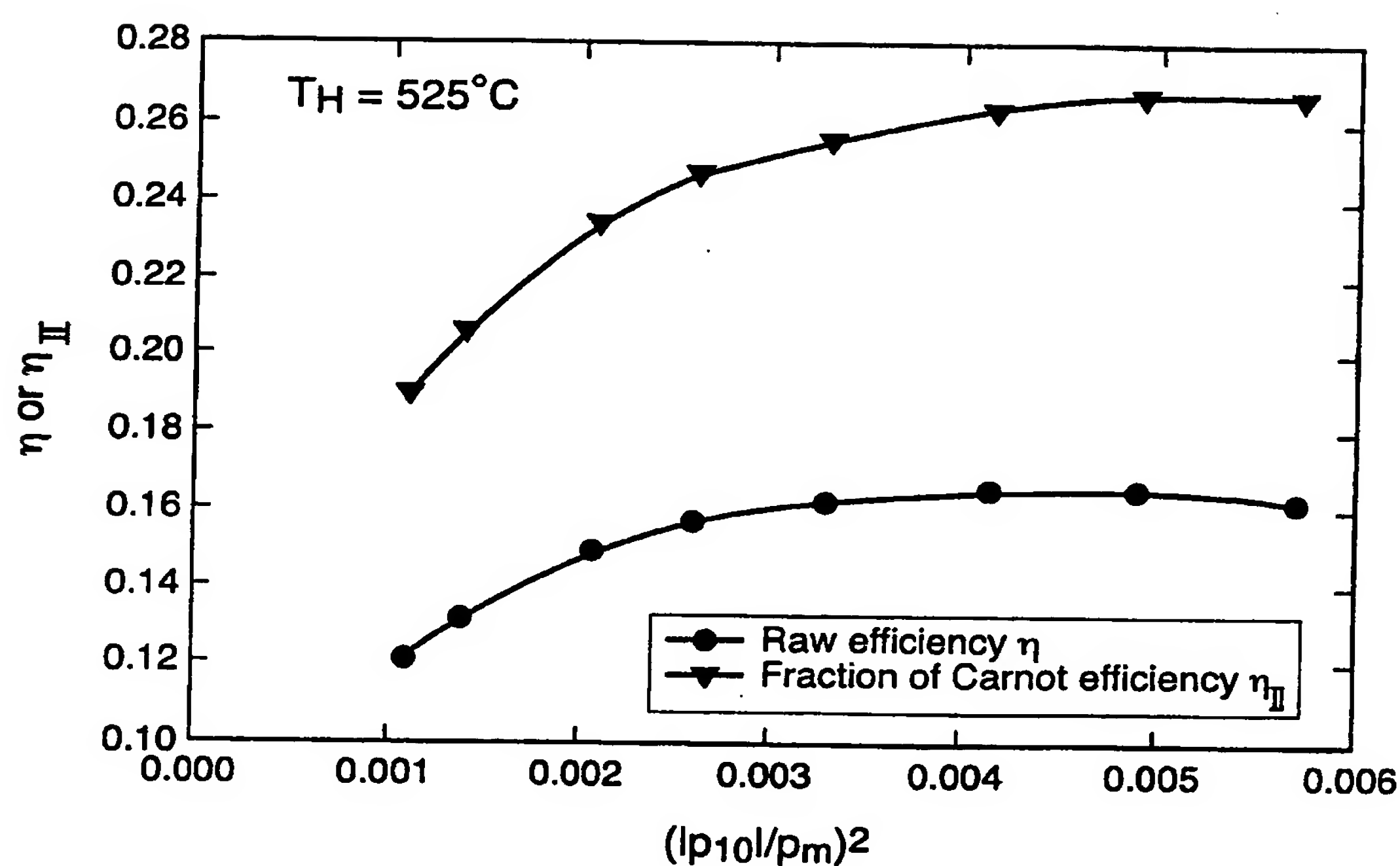


Fig. 11A

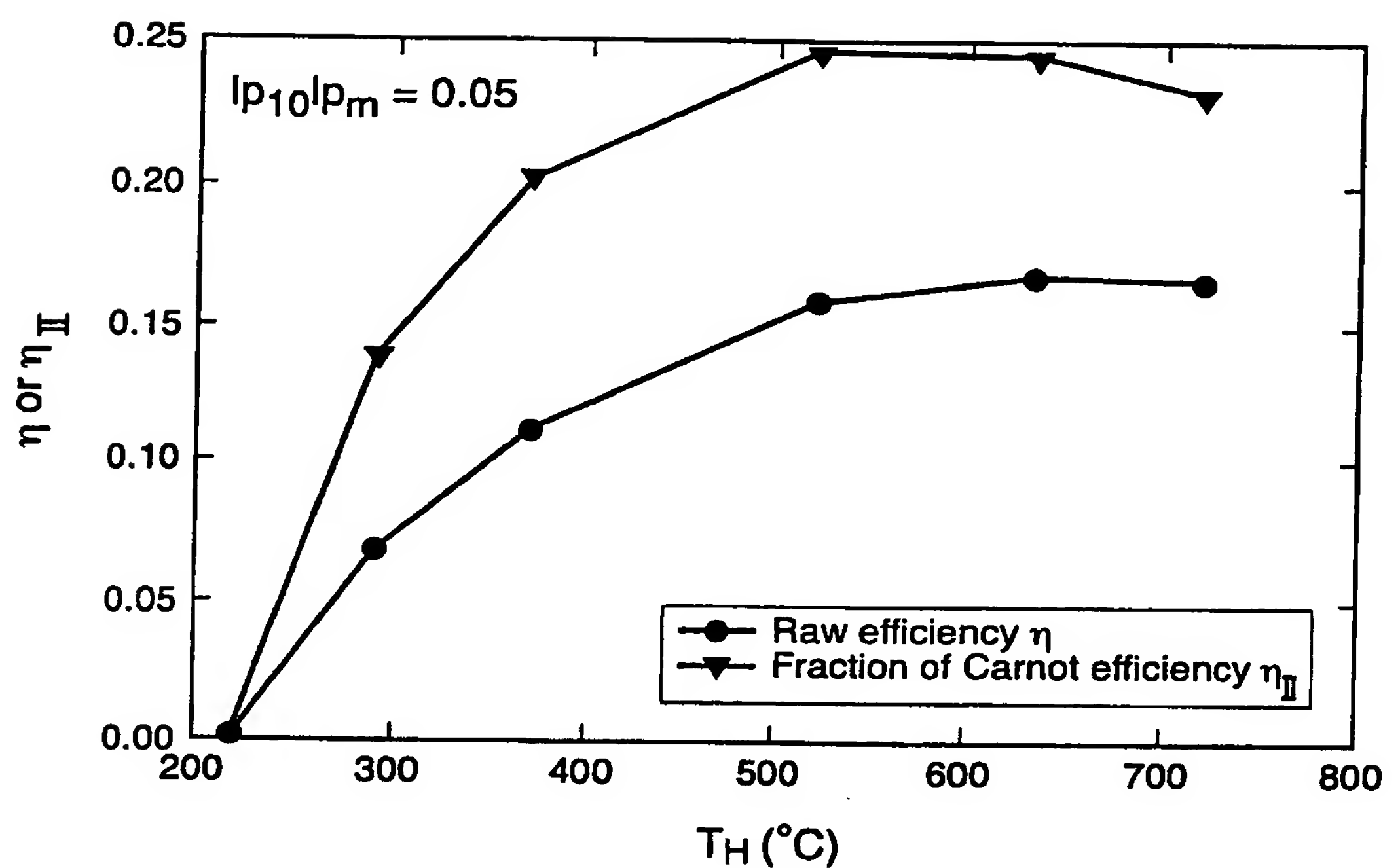
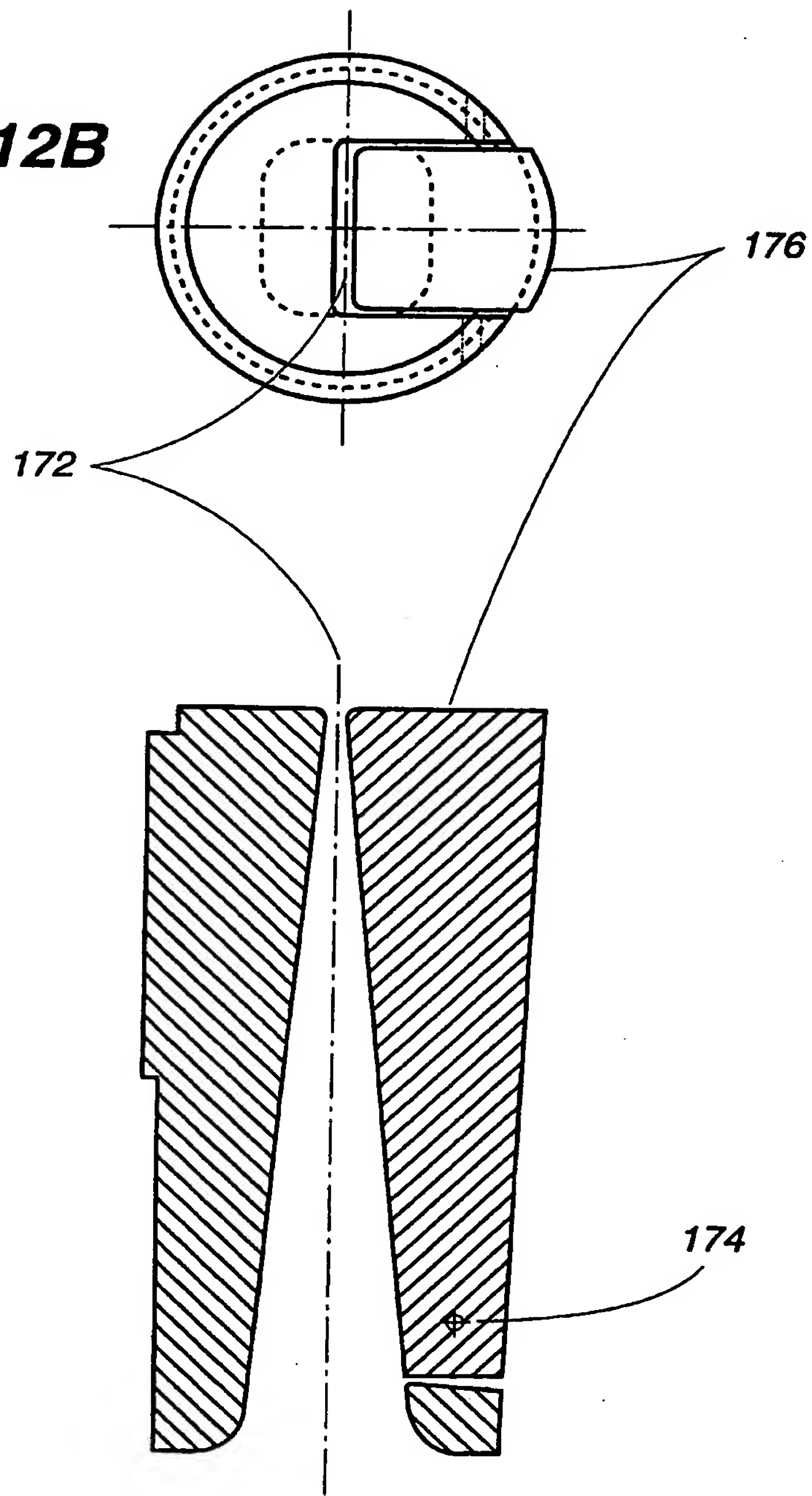


Fig. 11B

Fig. 12B***Fig. 12A***

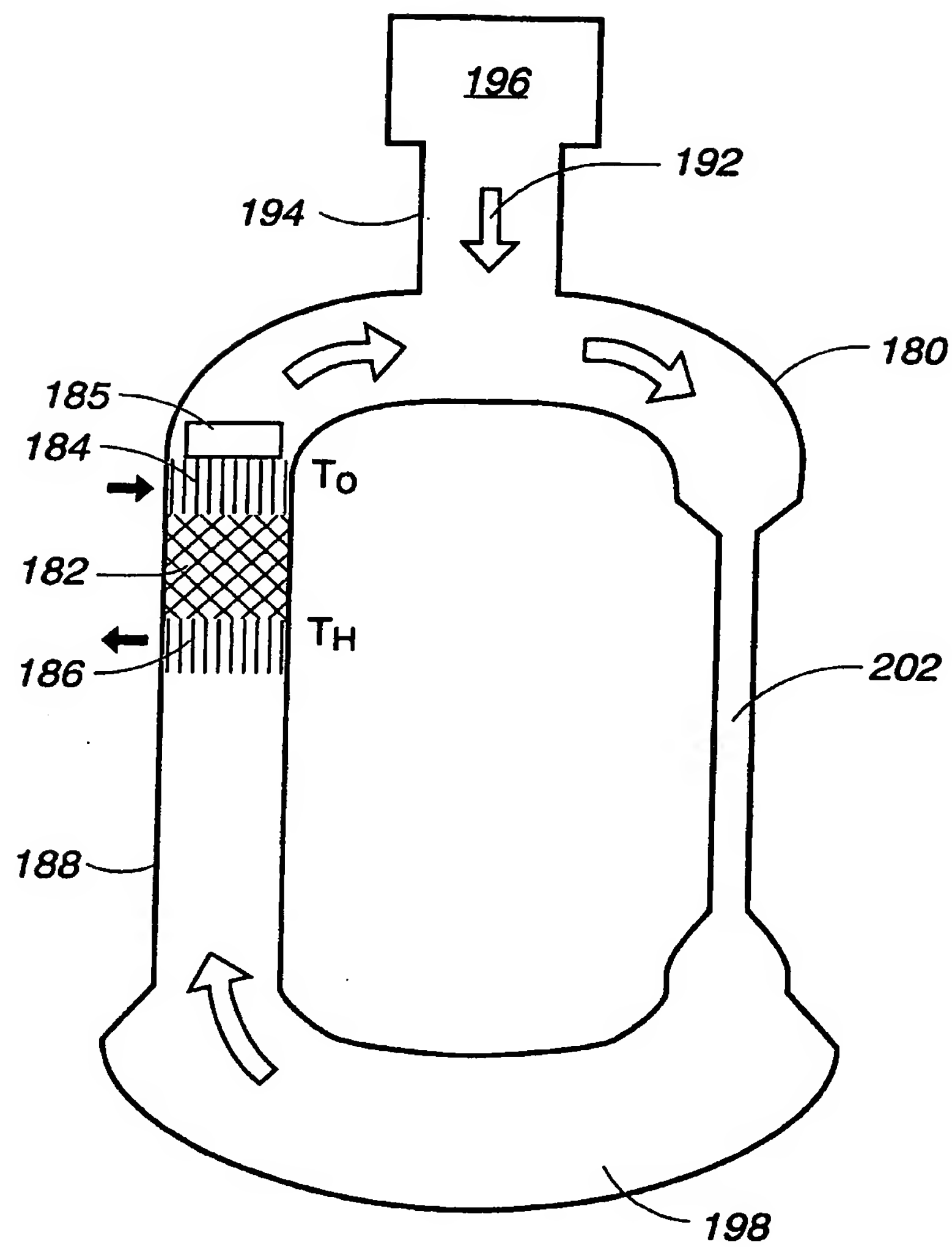


Fig. 13A

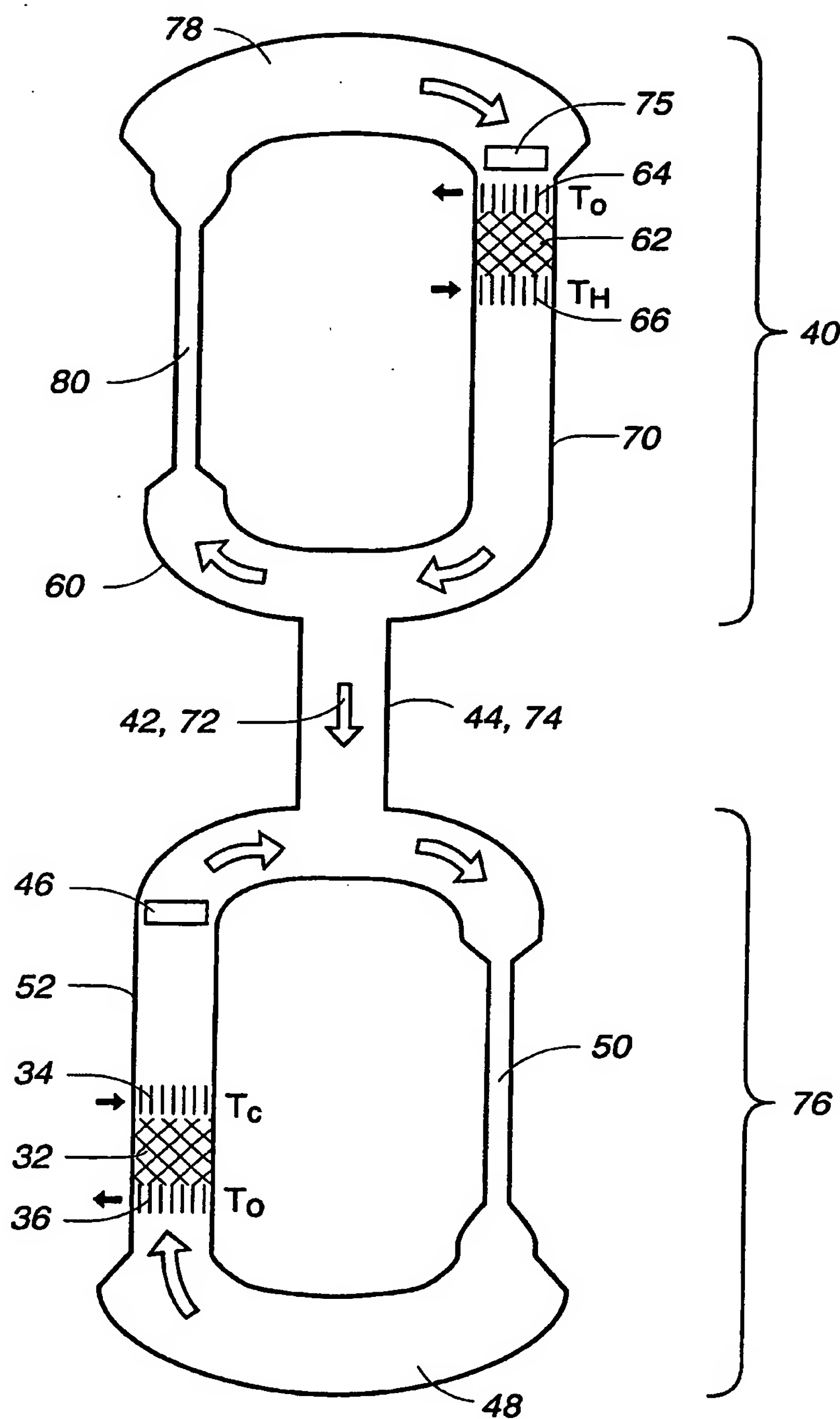


Fig. 13B

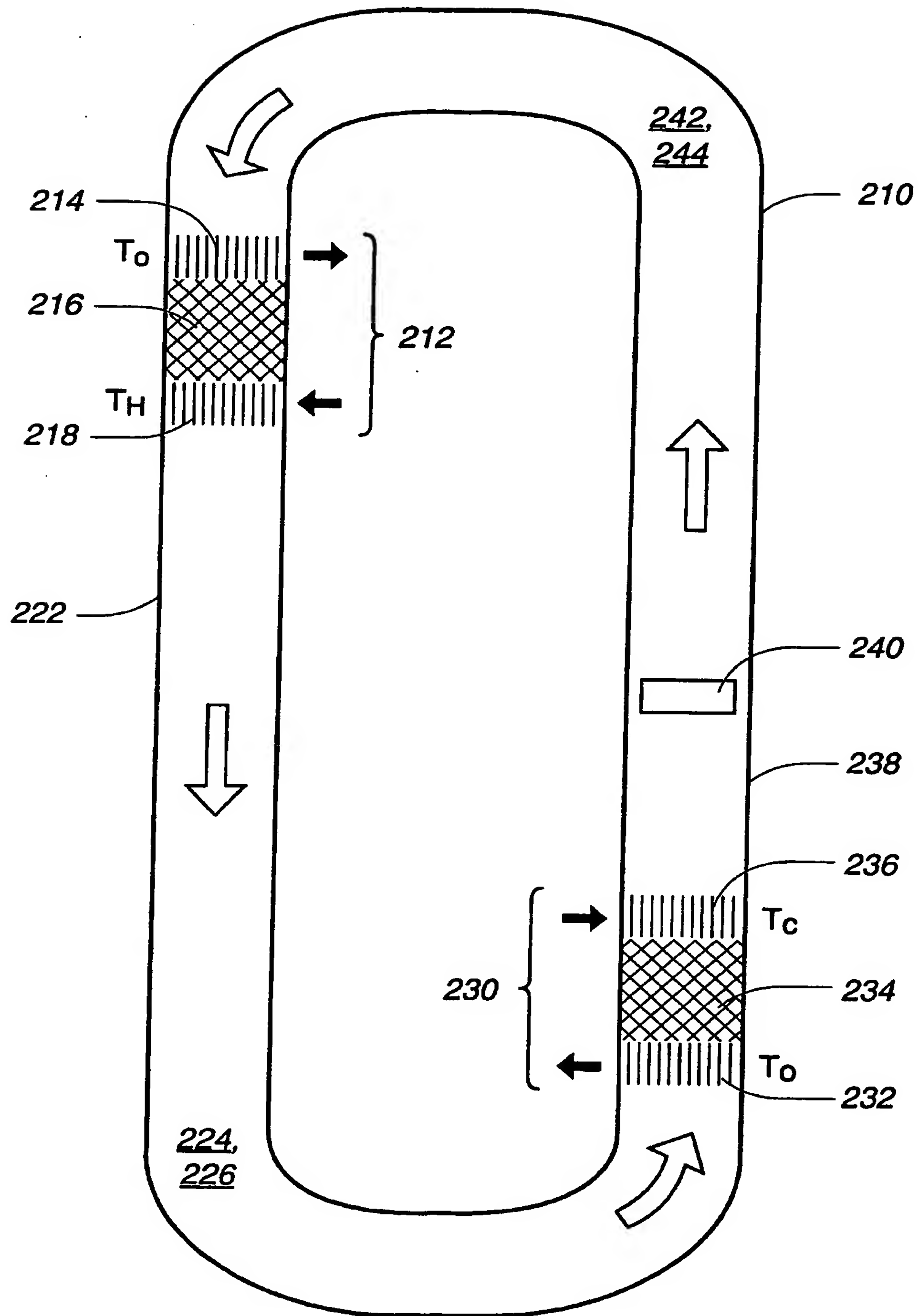


Fig. 13C

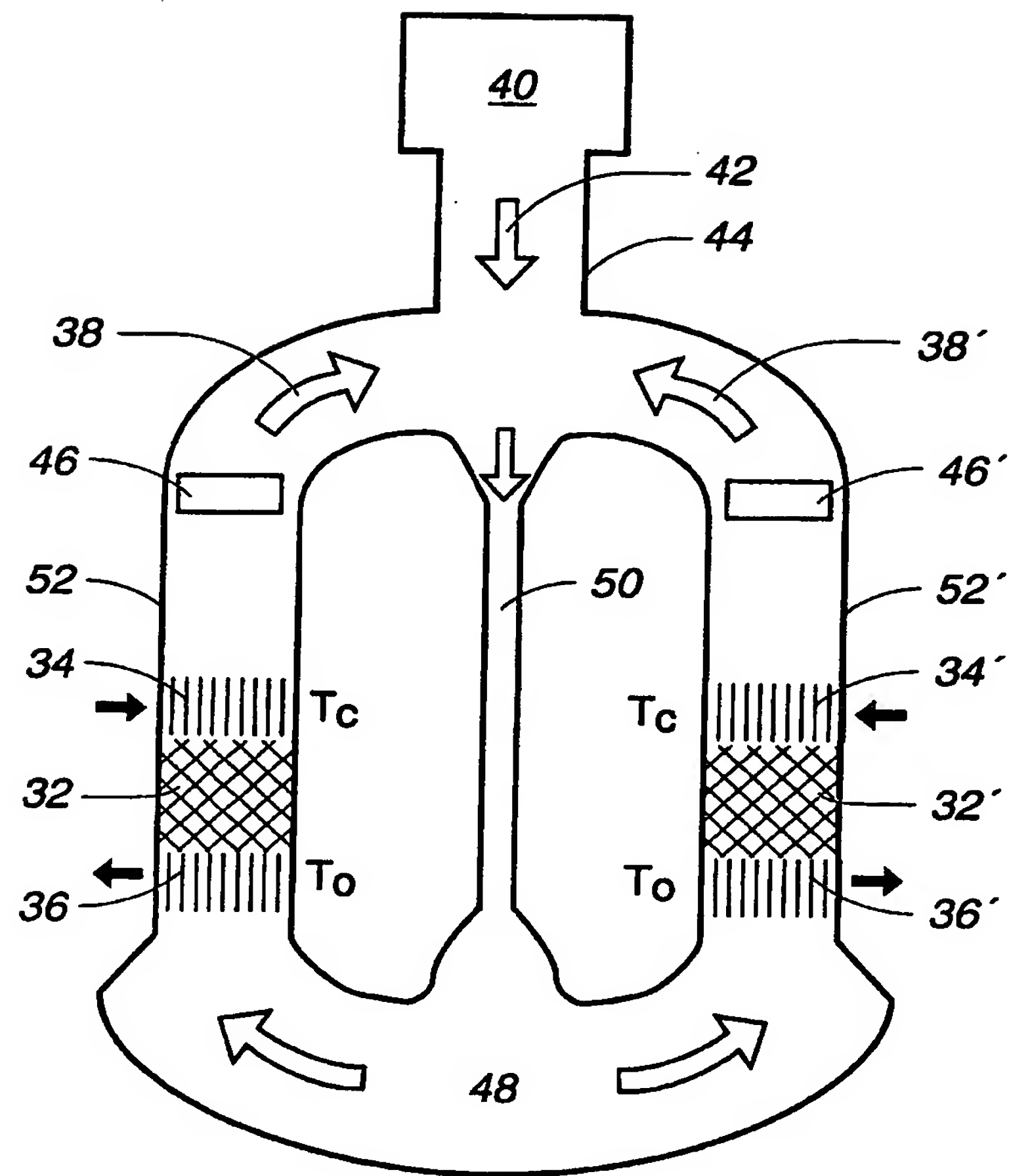


Fig. 13D

INTERNATIONAL SEARCH REPORT

International application No.
PCT/US00/01308

A. CLASSIFICATION OF SUBJECT MATTER

IPC(7) :F01B 29/10

US CL :60/521, 522

According to International Patent Classification (IPC) or to both national classification and IPC

B. FIELDS SEARCHED

Minimum documentation searched (classification system followed by classification symbols)

U.S. : 60/517, 521, 522, 526

Documentation searched other than minimum documentation to the extent that such documents are included in the fields searched
NONEElectronic data base consulted during the international search (name of data base and, where practicable, search terms used)
NONE

C. DOCUMENTS CONSIDERED TO BE RELEVANT

Category*	Citation of document, with indication, where appropriate, of the relevant passages	Relevant to claim No.
A	US 4,355,517 A (CEPERLEY) 26 October 1982, see figures 1-5.	1-22
A, P	US 5,953,920 A (SWIFT et al) 21 September 1999, see figure 2.	1-22
A	US 5,519,999 A (HARPOLE et al) 28 May 1996, see figure 10.	1-22

<input type="checkbox"/>	Further documents are listed in the continuation of Box C.	<input type="checkbox"/>	See patent family annex.
*	Special categories of cited documents:	"T"	later document published after the international filing date or priority date and not in conflict with the application but cited to understand the principle or theory underlying the invention
"A"	document defining the general state of the art which is not considered to be of particular relevance	"X"	document of particular relevance; the claimed invention cannot be considered novel or cannot be considered to involve an inventive step when the document is taken alone
"E"	earlier document published on or after the international filing date	"Y"	document of particular relevance; the claimed invention cannot be considered to involve an inventive step when the document is combined with one or more other such documents, such combination being obvious to a person skilled in the art
"L"	document which may throw doubts on priority claim(s) or which is cited to establish the publication date of another citation or other special reason (as specified)	"&"	document member of the same patent family
"O"	document referring to an oral disclosure, use, exhibition or other means		
"P"	document published prior to the international filing date but later than the priority date claimed		

Date of the actual completion of the international search 18 APRIL 2000	Date of mailing of the international search report 06 JUN 2000
Name and mailing address of the ISA/US Commissioner of Patents and Trademarks Box PCT Washington, D.C. 20231 Facsimile No. (703) 305-3230	Authorized officer HOANG MINH NGUYEN Telephone No. (703) 308-0861 <i>Stacia Cadmus</i> <i>ftr</i>